Revolutionizing Ultra-High-Performance Concrete: Unleashing Metakaolin and Diatomaceous Earth as Sustainable Fly Ash Alternatives

Meghana Yeluri[a], Elif G. Ertugral[b], Yashovardhan Sharma[a], Petru S Fodor[c], Chandrasekhar R. Kothapalli[b], Srinivas Allena[a, *]

[a]Department of Civil and Environmental Engineering, Cleveland State University, Cleveland, OH 44115, United States

[b]Department of Chemical and Biomedical Engineering, Cleveland State University, Cleveland, OH 44115, United States

[c]Department of Physics, Cleveland State University, Cleveland, OH 44115, United States

*Corresponding author E-mail address: s.allena@csuohio.edu

Abstract

Ultra-high-performance concrete (UHPC) incorporating supplementary cementitious materials (SCMs) presents a novel and promising material with remarkable mechanical and durability properties. However, the utilization of silica fume in such SCMs is hindered by its high cost while that of class F fly ash by its availability. Towards exploring alternative economical and eco-friendly SCMs, as well as reduce the quantity of silica fume and cement in UHPC, this study reports on the benefits of using metakaolin (MK) and diatomaceous earth (DE) as replacements for fly ash in non-proprietary UHPC blends. MK and DE were added to replace fly ash (FA), up to 100% in 25% increments, without changing the silica fume (SF) content. In separate mixtures, MK and DE were added 100% each to replace both FA and SF. The resulting mixtures were extensively characterized for their flow, rheological properties, compressive strength, flexural strength, split tensile strength, and modulus of elasticity, under two curing conditions. Scanning electron microscopy, BET surface area, and particle size analysis were performed to investigate the size and shape, surface area, and morphology of the cementitious powders. Results indicate that the addition of MK and DE resulted in increased apparent viscosity and shear stress with rising shear rate, while yield stress values decreased ($p < 0.05$). The flow curves of all the modified UHPC mixtures fitted well ($R^2 > 0.99$) with the linear Bingham Plastic, modified Bingham Plastic, and Herschel-Bulkley models. UHPC mixtures with 100% replacement of FA with MK and DE achieved compressive strength values of 139 MPa and 128 MPa, respectively. At 28 days, MK, DE, and MK-DE mixtures showed 3.5% – 10% higher compressive strengths than the control mixture ($p < 0.05$). MK-DE mixture showed compressive strength improvements of 9% and 17.5% over the control and DE-modified mixtures, respectively ($p < 0.05$). The greatest modulus of rupture (MOR) value of 10.9 MPa at 28 days was observed in the control mixture, while DE modified UHPC exhibited the lowest MOR values among all the cases. At net deflection of L/150, the MK-DE modified UHPC mixture exhibited the greatest toughness value of 52.5 Joules at 28 days, which is 5% greater than that in control UHPC mixture. Both MK and DE modified UHPC mixtures showed toughness values similar to the control UHPC mixtures at 28 days. In conclusion, the MK-DE modified UHPC mixtures that were prepared, without SF and FA, exhibited

characteristics comparable to the control mixture, showcasing potential alternatives for non-proprietary UHPC mixtures.

Keywords: UHPC; Alternative SCMs; Rheology; Mixture development; Experimental optimization, Mechanical properties.

1. Introduction

Ultra-high-performance concrete (UHPC) is an advanced construction material known for its exceptional mechanical properties, durability, and versatility, making it a key innovation in modern infrastructure development. It exhibits compressive strengths greater than 120 MPa, flexural strengths greater than 15 MPa, and excellent durability characteristics in terms of resistance to chloride penetration, freeze-thaw resistance, and resistance to sulfate attack [1, 2, 3]. As the demand for high-performance and sustainable infrastructure continues to rise, UHPC is set to shape modern construction, enabling a safer and more resilient built environment. UHPC is typically comprised of cement, fine sand, silica fume (SF), quartz flour, high-range water reducing admixtures (HRWRA), and steel fibers [4, 5]. It is used in diverse construction projects, including bridge decks, high-rise buildings, precast elements, and seismic-resistant structures. Beyond infrastructure applications, this material can also be used in nuclear applications such as encapsulating solid and liquid radioactive waste and disposal infrastructure [3, 6, 7]. These exceptional characteristics are achieved by enhancing homogeneity, eliminating coarse aggregate, optimizing particle packing density, refining microstructure, and integrating fibers. Its superior material properties have opened new possibilities in structural design, enabling the construction of thinner and more intricate elements with reduced maintenance requirements. However, UHPC faces challenges such as high initial cost and the limited availability of key constituents like steel fibers and SF in the United States. Aggregate costs are often increased due to the processing of high-quality sands, such as clean quartz, to achieve a precise gradation with a narrow particle size distribution [8]. Additionally, the high cement content in UHPC mixtures poses sustainability challenges due to the energy-intensive nature of cement production and its significant CO_2 emissions. Non-proprietary UHPC presents opportunities for enhanced sustainability and reduced initial cost by incorporating local aggregates, even those with suboptimal quality and natural particle size distributions. Additionally, non-proprietary UHPC can make use of cost-effective supplementary cementitious materials (SCMs) that are readily available locally, despite being of lower quality compared to the high-grade SCMs like SF used in proprietary UHPC formulations [8].

SF is the primary SCM in UHPC, comprising 5% to 25% of the binder volume [9]. SF enhances UHPC's particle packing density, improving workability due to its fine particle size. However, exceeding 10% SF by weight can significantly reduce workability due to its high surface area, leading to water and HRWRA absorption, particle agglomeration, and inhibition of cement reaction [10, 11]. With SiO_2 content above 90%, SF stimulates cement hydration and refines UHPC microstructure, enhancing mechanical strength and durability [12]. Despite its effectiveness, use of SF in UHPC mixtures is expensive compared to other SCMs since it is mostly imported in the United States [13]. The high quantities of cement and expensive SF significantly

increases the cost of UHPC and is less desirable from an environmental standpoint. Besides its higher cost, exposure to SF in occupational settings increases the risk of developing pulmonary diseases [14]. Therefore, exploring feasible alternatives to SF is crucial for UHPC production sustainability.

Several alternative SCMs commonly used in UHPC, in lieu of SF, include fly ash (FA), ground granulated blast furnace slag (GGBS), metakaolin (MK), and rice husk ash (RHA) [15, 16, 17, 18]. Among these, FA has gained significant recognition in the construction industry as a key SCM. Numerous researchers have formulated UHPC mixtures incorporating FA due to its potential to lower the environmental impact when substituted for cement [19, 20]. Despite a slight reduction in mechanical properties [21], FA-based UHPC improves workability [22], and particle packing, potentially enhancing durability [23]. However, the production of class F fly ash has experienced a significant decline recently due to the shift towards renewable energy technologies for electricity generation as well as decommissioning of coal-burning power stations. Consequently, the construction sector is grappling with difficulties in procuring a sufficient supply of FA for concrete manufacturing [24, 25]. Hence, it becomes imperative to identify an alternative SCM to FA to ensure sustainability.

One promising alternative is MK, produced by calcining kaolin clay. It is commonly utilized as a SCM in concrete, replacing 8% to 10% of cement, and enhancing concrete durability while reducing cement usage [26, 27]. MK reacts with calcium hydroxide during cement hydration, forming secondary calcium silicate hydrate (C-S-H) gel, enhancing concrete microstructure and durability by reducing porosity and improving permeability and chloride ion diffusion [28, 29]. Studies have shown MK can replace up to 20% of cement, improving compressive and split tensile strengths starting at 16% replacement. However, MK and SF addition decrease concrete workability. Yet, at 15% cement replacement, compressive strengths remain comparable to control samples (SF is the only SCM) after 91 days, exhibiting excellent corrosion resistance and reduced shrinkage [19]. Others have investigated various types of concretes and mortars replacing cement and SF with MK [30, 31, 32], but there is a lack of research specifically focused on UHPC incorporating MK to replace FA. This gap in the literature fails to highlight the beneficial impact of MK on the mechanical and durability properties of UHPC, as well as its contribution to the sustainability [33, 34].

Similarly, DE which is a natural pozzolan has emerged as a potential alternative SCM, given its high silica content. DE, a sedimentary and biogenic material, forms from the fossilization of algae shells due to silica deposits on diatom skeletons [38]. According to the U.S. Geological Survey, 2.3 million metric tons of DE were mined globally in 2021, with vast but currently unquantifiable reserves unexplored, and the United States produces approximately 36% of the world's supply [35, 36]. Its high open porosity (50% to 70%), large specific surface area, and high water absorption capacity (up to 1 kg/kg) make it useful in filtration, drilling mud thickening, and chromatography applications [37]. In cementitious materials, DE is often recommended for use in conventional and high performance concretes as a source of internal curing water and SCM [38, 39, 40, 41]. It is also used in fireproof cement, insulation materials, and as an absorbent in explosives due to its resistance to heat and chemicals [42]. The results from studies dealing with the use of DE as an

SCM replacing cement up to 10% by mass in UHPC mixtures are promising. Studies by Hasan et al. [38] and Du [41] reported that incorporating DE in UHPC and high performance concrete mixtures affected the flow, improved compressive, split tensile, and flexural strength. However, as current studies on its ability to enhance mechanical and durability performance are limited, further research is needed to elucidate the optimal use of DE as an SCM, particularly in UHPC formulations, to fully assess its potential benefits and drawbacks.

Thus, this study explored the potential for replacing FA and SF with cost-effective and environmentally friendly alternatives for UHPC mixtures. MK and DE were chosen as alternative SCMs to replace SF and FA due to their lower cost, reduced health risks, and promising performance in UHPC. SF, while effective, is expensive and poses health hazards due to its fine particulate nature, making MK and DE more sustainable, especially given the declining availability of FA and the need for environmentally friendly and cost-effective SCMs in UHPC formulations. The resulting rheological and mechanical properties of UHPC mixtures were evaluated and reported here. Additionally, the durability properties of UHPC modified with MK, DE, and MK-DE combinations are currently being investigated to assess their resistance to freezing-thawing cycles, chloride ion ingress, and sulfate attack. Preliminary observations suggest that the addition of MK and DE improves the durability of UHPC by enhancing resistance to chloride penetration and improving microstructural refinement.

2. Materials and Methods

2.1 Materials

Type 1L portland limestone cement (PLC) was utilized here. Class F FA was used as SCM along with SF in the control mixture. MK and DE were considered as alternatives for FA and SF. **Table 1** presents the physical and chemical properties of these materials. The particle size distributions on the as-received particles of the five precursors – cement, FA, MK, DE, condensed SF, were measured using a particle size analyzer (Anton Paar PSA 1190 model).

Local sand conforming to ASTM C33 [43] was used. Its specific gravity and absorption values determined as per ASTM C128 [44] were found to be 2.78% and 2.35%, respectively. Sand was sieved through ASTM No. 4 sieve (maximum particle size of (4.75 mm) and was oven-dried at 110 °C to achieve 0% moisture content. To enhance the tensile ductility of the UHPC, straight steel fibers measuring 13 mm in length, with an aspect ratio of 65, were used. To attain the desired workability, a commercially available polycarboxylate-based high-range water-reducing admixture (HRWRA; Master Builders Solutions, Cleveland, OH, USA) was added into the mixtures.

2.2 Development of UHPC mixtures

2.2.1. UHPC mixtures

Control UHPC mixture was developed using cement, SF, and FA as cementitious materials. Several trial batches were made to optimize the SF/FA ratio that would produce UHPC class material as defined by ASTM C1856 [45]. In these trials, different water-to-cementitious ratios (w/cm) and HRWRA dosages were used for a specific SF/FA ratio.

Table 1. Chemical composition and physical properties of cementitious materials used in this study.

		Materials Composition (%)				
		Cement Type IL (PLC)	Class F Fly Ash	SF	MK	DE
Chemical Composition	CaO	63.1	3	0.7785	-	1.24
	SiO_2	18.9	45.8	83.85	49.35	82.16
	Al_2O_3	4.4	22.8	0.56	45.03	4.85
	Fe_2O_3	2.5	22.6	3.63	0.5	1.66
	MgO	1.6	0.8	4.74	-	0.45
	Na_2O	0.34	0.47	-	-	0.54
	K_2O	-	1.76	1.12	0.42	0.72
	TiO_2	-	-	-	2.19	0.24
	MnO	-	-	0.3	-	0.01
	P_2O_5	-	-	-	0.097	0.06
	SrO	-	-	0.02	0.02	0.02
	Br	-	-	0.74	0.7	
	BaO	-	-		-	0.03
	SO_3	3	0.86	0.06	0.05	-
	Cr_2O_3	-	-	0.05	-	0.01
	Limestone	12.1	-	-	-	-
	CO_2	5.4	-	-	-	-
	$CaCO_3$	91	-	-	-	-
	Loss of Ignition	5.4	1.9	2.96	0.83	7.41
Physical Properties	Specific Gravity	3.15	2.48	2.2	2.5	2.2
	Specific Surface area (m^2/kg)	549.4	575.7	25,000	22,000	908.2
	Mean Particle Size (μm)	14.951	15.786	9.814	10.738	14.488
	Autoclave Expansion (%)	0.022	0.02	-	-	-

Preliminary tests such as workability and compressive strength were performed for each trial mixture and the optimum w/cm and SF/FA ratios, and HRWRA dosage were found to be 0.2, 1, and 34.65 L/m^3, respectively. Based on these results, UHPC mixture with 16% SCM - 8% SF -

8% FA by mass of cementitious materials, 0.2 w/cm ratio, 1.52% by total volume of steel fibers, and 34.65 L/m^3 HRWRA was selected as control mixture in this research. **Figure 1** depicts the mixture development process.

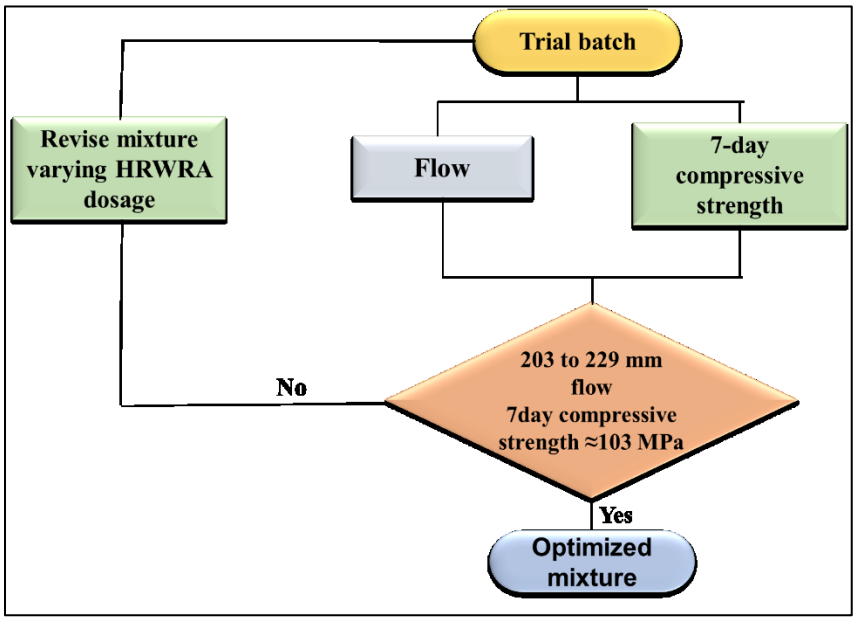

Figure 1. Optimization process of UHPC mixtures used in this study.

Table 2 presents the 10 UHPC mixture proportions developed in this study. Given our primary objective of substituting FA and SF with alternative SCMs, the control UHPC mixture with FA and SF are the SCMs were further modified. MK and DE were employed to replace FA incrementally, up to 100% in 25% increments, without changing the SF content. This process aimed to identify the optimal level of FA replacement. Subsequently, once the ultimate FA replacement levels with both MK and DE were established, the SF content was also modified utilizing MK and DE.

Table 2. Mixture proportions for UHPC mixtures developed in this study. The letters indicate the SCM type in the mixture, FA for fly ash, SF for silica fume, MK for metakaolin, and DE for diatomaceous earth.

Mixture		PLC	SF	FA	MK	DE	Sand	Steel Fibers	Water	HRWRA	w/cm	Flow
		kg/m^3	kg/m^3	kg/m^3	kg/m^3	kg/m^3	kg/m^3	kg/m^3	kg/m^3	l/m^3		mm
Control UHPC	SF8-FA8-MK0/DE0	890	89	89	0	0	939.7	118.7	213.6	34.65	0.2	254.0
MK Modified UHPC	SF8-FA6-MK2	890	89	66.7	22.24	0	950.7	118.7	209.0	34.65	0.2	228.6
	SF8-FA4-MK4	890	89	44.5	44.5	0	935.6	118.7	204.7	44.6	0.2	228.6
	SF8-FA2-MK6	890	89	22.24	66.7	0	946.6	118.7	200.2	44.6	0.2	228.6
	SF8-FA0-MK8	890	89	0	89	0	944.5	118.7	195.8	49.5	0.2	228.6
DE Modified UHPC	SF8-FA6-DE2	890	89	66.7	0	22.24	934.5	118.7	209.0	39.6	0.2	215.9
	SF8-FA4-DE4	890	89	44.5	0	44.5	929.2	118.7	204.7	44.6	0.2	215.9
	SF8-FA2-DE6	890	89	22.24	0	66.7	924.1	118.7	200.2	49.5	0.2	215.9
	SF8-FA0-DE8	890	89	0	0	89	867	118.7	195.8	74.3	0.2	215.9
MK-DE Modified UHPC	SF0-FA0-MK8-DE8	890	0	0	89	89	879.7	118.7	195.8	74.3	0.2	215.9

UHPC mixtures belonging to each category were assigned specific designation based on their composition. The number following each letter indicates the percentage of the SCM in the mixture. For instance, the control mixture SF8-FA8-MK/DE0 contained 8% of SF and 8% of FA out of total cementitious materials and in the case of mixture SF8-FA6-MK2, 25% of FA was replaced with MK, resulting in a mixture that contains 6% FA and 2% MK out of total cementitious materials content.

To achieve a homogenous UHPC mixture with uniform dispersion of fibers, a step-by-step mixing process was employed (**Figure 2**). A vertical shaft mixer with a 38-rpm paddle speed was used to mix the constituents of UHPC. The procedure commences with a two-minute mixing of the dry components, followed by the gradual addition of two-thirds of the required water, and mixed for an additional three minutes. Subsequently, HRWRA and the remaining portion of water were introduced, and mixed for another three minutes. At the end, steel fibers were added during the mixing process. The total mixing time varied from 15–20 min. The fresh UHPC was then poured into molds and covered with plastic sheets to prevent moisture loss. They were then left at room temperature for 24 h. Following this period, the specimens were removed from the molds and subjected to designated curing conditions as described in section 2.2.3.

2.2.2 Specimen preparation

Each batch of UHPC produced was used to cast 50 mm and 100 mm cubes for compression testing, 75 mm × 100 mm × 400 mm beams for flexural testing, and 100 mm × 200 mm cylinders for split tensile testing and modulus of elasticity measurements. A high frequency vibration table was used for consolidation. The time of vibration was selected based on the consistency of the individual mixture that ranged between 15 sec to 30 sec.

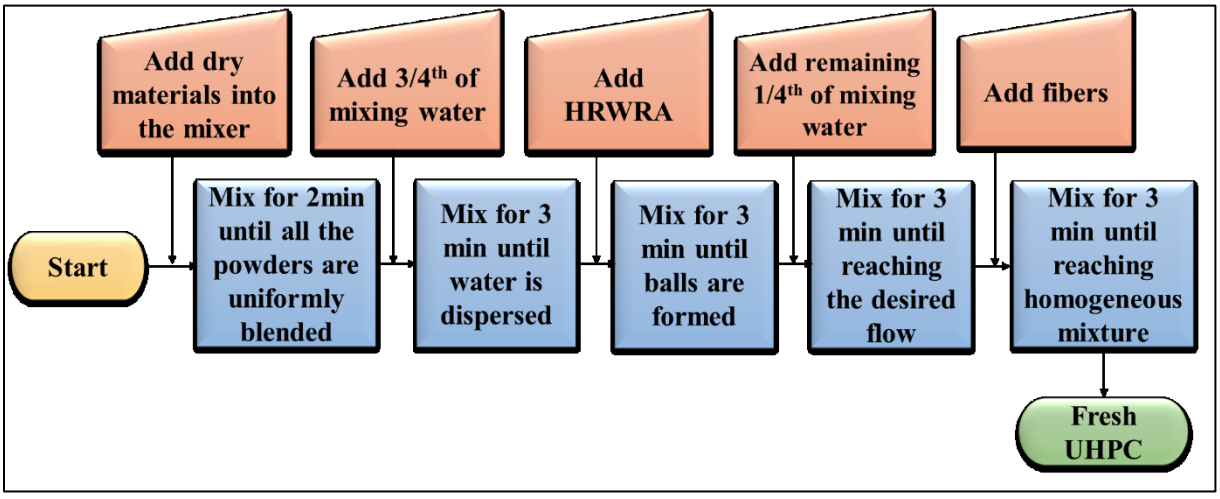

Figure 2. Mixing sequence for the UHPC constituents used in this study.

2.2.3 Curing regimens

Specimens were cured under the two curing regimens (**Table 3**) to investigate the effect of curing temperature on mechanical properties.

214 **Table 3.** Curing Regimens used in this study.

Curing condition	Specification
Moist curing (MC)	Air cured in the molds for 24 h. After demolding, the specimens were placed in a moist room with ~100% relative humidity and temperature 23.5 ± 1.5 °C until the day of testing.
Warm bath (WB)	Air cured in the molds for 24 h. After demolding, specimens were cured in a water bath at 90 °C until the time of testing. This curing method simulated the steam curing method employed in precast plants.

215

216 ## 2.3 Experimental methods

217 ### 2.3.1 Particle size distribution and surface area

218 Anton-Paar Model PSA 1190 particle size analyzer (using dry jet dispersion and laser diffraction
219 techniques) was used to determine the particle size distributions. Cement and FA were analyzed
220 using dry measurement mode. The detection limit of this mode is 0.1 μm. SF, DE, and MK were
221 analyzed using liquid measurement mode with small volume unit. The detection limit of this mode
222 is 0.04 μm. Anton Paar Nova 600 BET analyzer was used for surface area measurement of cement,
223 SF, FA, MK, and DE.

224 ### 2.3.2 Flow table test

225 Fresh UHPC was poured into the mold in two layers, with each layer being tamped 20 times.
226 Following this, the top surface was smoothened. The mold was then lifted and immediately
227 dropped onto the table 25 times within a 15-second period. Subsequently, the diameter of the fresh
228 sample was measured in two diametrically opposite directions, and the average flow recorded as
229 outlined in ASTM C1437 [46].

230 ### 2.3.3 Compressive strength testing

231 In this study, four 50 mm cube specimens and two 100 mm cube specimens, cured under MC and
232 WB regimens, were tested at each age (3, 7, 28, 56, and 91 days), according to ASTM C109 [47]
233 and average compressive strength reported.

234 ### 2.3.4 Flexural strength testing

235 75 mm × 100 mm × 400 mm prismatic specimens were cast from each batch of UHPC and cured
236 under MC and WB regimens. Flexural strength tests were conducted at ages 7 and 28 days in
237 accordance with ASTM C1609 [48]. Three prismatic specimens were tested at each age. Strengths
238 and deflections at first peak load, peak load, residual strengths at net deflections of span/600 and
239 span/150 (f_{600}^{D} and f_{150}^{D}), and toughness values corresponding to net deflections of span/600
240 (T_{600}^{D}) and span/150 (T_{150}^{D}) were determined.

241

242

2.3.5 Split tensile strength testing

100 mm × 200 mm cylinder specimens were cast from each batch and moist cured until 28 days and were tested for split tensile strength according to ASTM C496 [49]. Two-cylinder specimens from each batch were tested and average split tensile strength was reported.

2.3.6 Modulus of elasticity testing

100 mm × 200 mm cylinder specimens cured for 28 days in MC regimen were subjected to axial compressive loading to determine the modulus of elasticity and Poisson's ratio according to ASTM C469 [50].

2.3.7 Rheology tests on cement paste

Rheology tests on aggregate-free cement pastes were performed to assess viscosity, shear stress, shear thickening, and shear thinning behavior in UHPC mixtures. The pastes were characterized at room temperature using a Physica MCR 301 Rheometer (Anton Paar, Ashland, VA) using a concentric cylindrical geometry (CC27, 26.66 mm diameter) with smooth surfaces. After the cement pastes were loaded in the cup, they were pre-sheared at 10^2 s^{-1} for one minute, rested for five minutes, followed by a constant shear rate of 1 s^{-1} for one minute, and then rested again for five minutes. Viscosity (η, Pa.s) measurements were performed by setting the shear rate within 1 – 100 s^{-1} range. Shear stress vs. shear rate curves were evaluated to determine the paste characteristics.

2.3.8 Thermogravimetric analysis

Thermogravimetric analysis (TGA) was conducted using a TGA/DSC 3+ thermogravimetric analyzer (Mettler Toledo) under nitrogen atmosphere. The temperature range for all samples was set from 30 °C to 900 °C at a constant heating rate of 10 °C/min. This analysis was performed to evaluate the thermal stability and mass loss characteristics of the cementitious materials.

2.3.9 Scanning electron microscopy

Scanning electron microscopy (SEM) imaging was systematically carried out on dry cementitious powders. The primary objective was to meticulously explore and analyze the distinct microstructure inherent to each individual material. This detailed examination provided valuable insights into the fine-scale features such as particle shape and morphology of the cementitious powders under consideration. SEM imaging was performed using a field emission scanning electron microscope (FEI, model Inspect F50) equipped with an Everhart-Thornley detector. The dry powder samples were affixed to the aluminum specimen mounts using conductive carbon tape. Prior to imaging, the samples were gold coated using a vacuum-based sputter coater (SPI Sputter Coater from SPI Supplies Inc.) to prevent electrostatic charging of the surface during imaging.

2.4. Statistical analysis

At least n = 3 samples were used per test unless otherwise noted. Results were plotted using GraphPad Prism 10 software. A one-way ANOVA with post hoc Tukey's test was used for comparisons of the results from multiple experiments, with statistical significance set at $p < 0.05$.

3. Results and Discussion

3.1. Thermogravimetric analysis of cementitious materials

Thermogravimetric analysis was performed on cement, SF, FA, MK, and DE and the result was depicted in **Figure 3**.

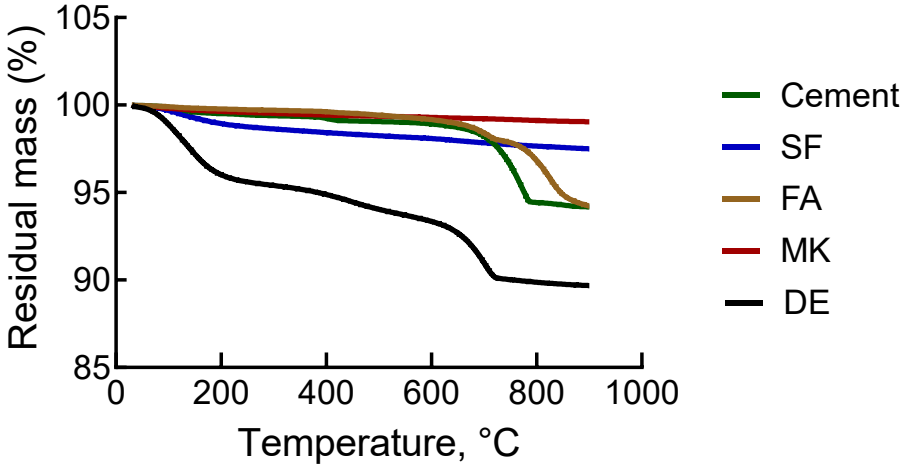

Figure 3. Thermogravimetric analysis of dry cement, SF, FA, MK, and DE

Cement exhibited a residual mass of 94% at 900 °C, with approximately 6% mass loss primarily occurring in two stages. The initial minor loss below 200 °C can be attributed to the evaporation of free and physically absorbed moisture. The major mass loss between 400 °C and 550 °C corresponds to the decomposition of calcium hydroxide (CH) into calcium oxide (CaO) and water, while further decomposition of calcium carbonate ($CaCO_3$) to CaO and CO_2 takes place above 600 °C. This decomposition profile highlights the stability of cement up to high temperatures, while its thermal transformations are crucial for hydration reactions in UHPC systems. SF demonstrated the highest thermal stability among the analyzed materials, retaining 97.5% residual mass at 900 °C. The minimal mass loss reflects its chemically inert nature and lack of decomposition products. The slight mass loss below 200 °C can be linked to surface-adsorbed moisture, while no significant decomposition occurs at higher temperatures. This stability, combined with its fine particle size and high amorphous silica content, makes SF a key pozzolanic material for enhancing the microstructure of UHPC.

FA retained 94% residual mass, showing gradual mass loss across the temperature range. The initial loss below 200 °C is due to the evaporation of moisture, while minor losses observed between 300 °C and 500 °C could result from the decomposition of carbonaceous impurities and other volatile components. FA's moderate thermal stability and pozzolanic reactivity arise from its glassy phases, which contribute to strength development in UHPC. Metakaolin exhibited the highest residual mass, retaining 99% at 900 °C. The primary mass loss occurred below 400 °C, can be attributed to the dehydroxylation of kaolinite, where chemically bound water is released as

the material transforms into an amorphous aluminosilicate. The absence of significant decomposition at higher temperatures highlights the exceptional thermal stability of MK, while its high reactivity makes it an attractive SCM for UHPC applications. However, while MK can complement FA, its characteristics suggest it is better suited to replace SF rather than FA, as its high reactivity and fine particle size align more closely with SF's role in refining UHPC microstructure.

DE showed the lowest residual mass, retaining 89.7% at 900 °C, with significant mass loss occurring between 100 °C and 500 °C. This behavior is attributed to the release of adsorbed water and decomposition of organic impurities. The residual mass beyond 500 °C reflects the thermal stability of its silica framework. Although DE exhibits the highest mass loss, its high silica content and porous structure suggest potential reactivity, especially when processed or modified to enhance its performance.

The TGA analysis highlights significant differences in thermal stability and decomposition behavior among the materials. SF and MK demonstrated the highest stability, with MK's dehydroxylation indicating superior pozzolanic reactivity. FA showed moderate stability and reactivity, while DE's high mass loss reflects lower stability but suggests potential as a reactive SCM due to its silica content. Based on these observations, MK is an excellent candidate to replace SF in UHPC, while DE could serve as a sustainable alternative to FA when properly engineered to optimize its performance.

3.2. Rheology of pastes containing different cementitious materials

Representative SEM images of the milled dry powder samples and cumulative size distribution analysis of the particles obtained from particle sizing is shown in **Figure 4**. The SEM images allow the visualization with submicrometer precision of the morphology of the SCMs used in this study, giving insights on the particles' shape, surface structure, and geometrical parameters distribution. Based on the distribution analysis the average particle sizes were 14.951 μm, 14.488 μm, 15.786 μm, 10.738 μm, and 9.814 μm for PLC, DE, FA, MK, and SF, respectively. Similarly, the specific surface area of the particles were 549. 4 m^2/kg, 908.2 m^2/kg, 575.7 m^2/g, 22,000 m^2/kg, and 25,000 m^2/kg for PLC, DE, FA, MK, and SF, respectively. All the particles sizes followed normal distribution.

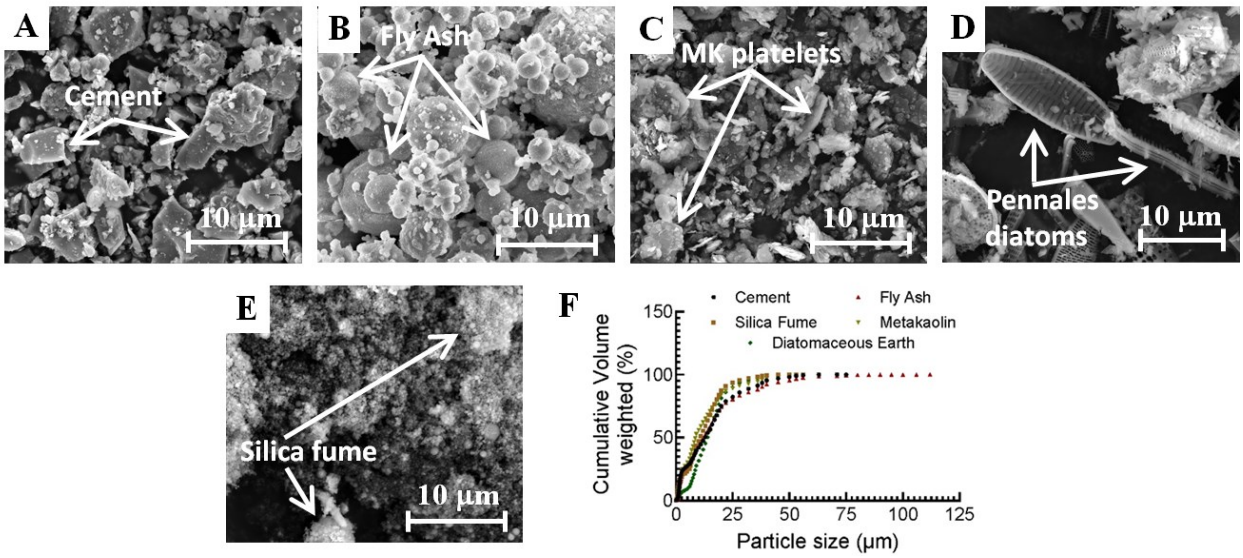

Figure 4. Representative SEM images of raw materials indicating representative particles of (A) cement, (B) FA, (C) MK, (D) DE, and (E) SF. (F) The cumulative particle size distribution for each of these types of particles.

The shear stress vs. shear rate data were obtained from the flow curves obtained on these four pastes – control, MK, DE, and MK-DE. These samples correspond to compositions described in Table 2, i.e., SF8-FA8-MK0-DE0, SF8-FA0-MK8-DE0, SF8-FA0-MK0-DE8, and SF0-FA0-MK8-DE8, respectively. The trends are represented in the shear stress vs. shear strain rate plots shown in **Figure 5**. The data were fit to the commonly used [51] two-parameter linear Bingham plastic model given by Eq (1):

$$\tau = \tau_0 + \mu_P \dot{\gamma} \qquad (1)$$

where τ_0 (Pa) is the yield stress that the paste needs to overcome before it flows and μ_P is the sample apparent viscosity (Pa.s). Expectedly, the model fitted very well to the data, as evident from the R^2 values (**Table 4**). It could be seen that the sample apparent viscosity increased when MK or DE was added to the control samples to completely replace FA, or when both MK and DE were added to completely replace SF and FA. In contrast, the yield stress values decreased with the addition of MK, DE, or both MK and DE.

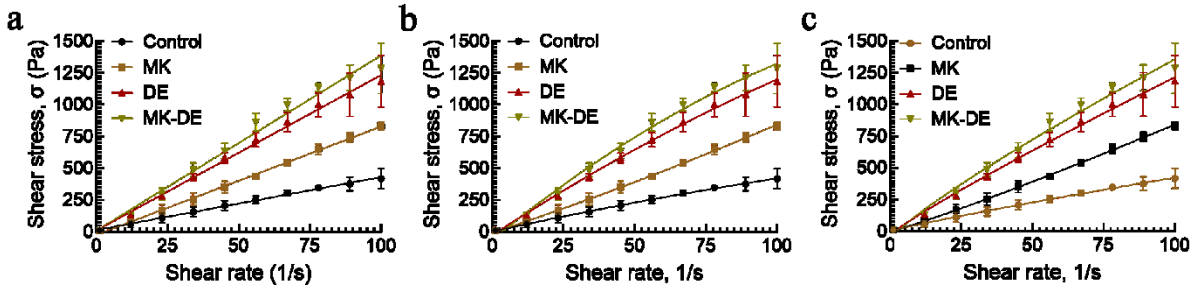

356

357 **Figure 5.** Shear stress vs. shear rate plots for the four pastes – controls, MK, DE, and MK-DE,
358 corresponding to SF8-FA8-MK0-DE0, SF8-FA0-MK8-DE0, SF8-FA0-MK0-DE8, and SF0-FA0-
359 MK8-DE8, respectively, whose compositions were shown in Table 2. The data were fit to three
360 different models: (a) a linear Bingham Plastic model, (b) a quadratic modified Bingham Plastic
361 model, and (c) a Herschel-Bulkley model.

362

363 **Table 4.** Parameters from the three models fitted to the shear stress vs. shear rate data from
364 rheological studies on respective pastes. In all the cases, $R^2 > 0.98$ indicating the strength of the
365 fit, with all model parameters also being significant ($p < 0.001$).

		Control	MK	DE	MK-DE
Bingham Plastic Model	τ_0, Pa	15.69	13.54	12.65	10.6
	μ_p, Pa.s	4.161	8.514	12.22	13.78
	R^2	0.99	0.99	0.99	0.98
Modified Bingham Plastic Model	τ_0, Pa	4.245	-6.175	-24.39	-58.85
	μ_p, Pa.s	4.906	7.449	14.63	18.3
	C	-0.0073	-0.0105	-0.0238	-0.0447
	R^2	0.99	0.99	0.99	0.99
Herschel-Bulkley Model	τ_0, Pa	1.415	1.223	-26.1	-58.01
	A, Pa.s	6.854	5.221	19.44	27.58
	n	0.8955	1.104	0.9027	0.8551
	R^2	0.99	0.99	0.99	0.98

366

367 Since the viscosity vs. shear strain rate data could exhibit shear-thinning or shear-thickening
368 behavior for fresh cementitious pastes, the apparent viscosity would not remain constant, which
369 indicates a non-linear relationship between the shear stress and shear strain rate under steady flow
370 state. To accurately describe the non-linear rheological behavior of fresh pastes, the shear stress-
371 shear strain rate curves were fitted to a modified Bingham plastic model based on a 3-parameter
372 quadratic equation, and the Herschel–Bulkley model containing an exponential term [52, 53, 54,
373 55, 56, 57, 58], given by equations (2) and (3), respectively:

374 $$\tau = \tau_0 + \mu_P \dot{\gamma} + C\dot{\gamma}^2 \quad (2)$$

where τ_0 (Pa) is the yield stress that the paste needs to overcome before it flows, μ_P is the sample viscosity (Pa.s) and C (Pa.s^2) is the coefficient of a second-order correction term in the shear strain rate. It is worth noting that $C > 0$ indicates shear thickening, $C < 0$ indicates shear thinning, and $C = 0$ results in linear Bingham plastic model described in Eq (1). The modified model fitted very well to the data, as evident from the R^2 values (**Table 4**). For the cementitious pastes developed here, C was less than zero for all the samples. The sample viscosity steadily increased when MK or DE or both MK and DE were added to the control samples. In contrast, the yield stress values steadily decreased with the addition of MK, DE, or both MK and DE.

$$\tau = \tau_0 + A\dot{\gamma}^n \quad (3)$$

Where τ_0 (Pa) is the yield stress that the paste needs to overcome before it flows, A is the sample consistency coefficient (Pa.s) and n is the flow behavior index. If n = 1, the Herschel-Bulkley model equals to the linear Bingham Plastic model described in Eq (1). The Herschel-Bulkley model also fitted well to the data, as evident from the R^2 values (**Table 4**). For the pastes developed here, n varied between 0.8551 to 1.104, whereas A values steadily increased when DE alone or both MK and DE were added to the control samples. In contrast, the yield stress values steadily decreased with the addition of MK, DE, or both MK and DE.

The apparent viscosity was in the order: control < MK < DE < MK + DE, whereas the yield stress was in the order: control > MK > DE > MK + DE. All the samples exhibited shear-thinning behavior with increasing shear rate. In the control sample, the cement pastes at rest require large stress to break the 3D structure formed between FA, SF and other ingredients, and thus exhibited higher yield stress. Once the structure was broken down, the paste flowed easily as indicated by low apparent viscosity and shear thinning behavior. MK addition (to replace FA) likely led to higher water absorption of the layered compounds (alumina and silica) in MK that induces flocculation of the paste [59] , thus increasing the apparent viscosity while reducing the yield stress, compared to control pastes. DE is a highly porous fossilized matter containing mostly silica, with high surface to weight ratio and abundant Si-OH groups, and acts mostly as a filler in the cement paste [60, 61]. DE might react with the calcium hydroxide in the mixture to form calcium silicate, which lowers the flowability of the paste upon shear [62]. Due of this, it contributes primarily to increase in apparent viscosity, with little impact on yield stress, unlike MK. Finally, the pastes containing both MK and DE which replaced SF and FA, exhibited the lowest yield stress and highest apparent viscosity most likely due to the nature of these two compounds acting primarily as fillers.

3.3 Optimization of UHPC mixtures

The control mixture described in section 2.2.1 served as the baseline for further optimization. This involved substituting FA with MK and DE, as well as replacing SF with MK in the DE-modified UHPC mixture. Final mixtures were identified based on the flow and seven-day compressive strengths.

3.3.1 Metakaolin as SCM to replace fly ash

The process aimed to reduce FA content by replacing it with MK at levels from 0% to 100% in 25% increments. **Figure 6** depicts the impact of MK content on the HRWRA dosage and seven-day compressive strengths of UHPC mixtures cured under MC and WB regimens. As MK increased, UHPC flow decreased, requiring increased HRWRA dosage to maintain the target flow of 203.2 mm to 228.6 mm (**Figure 6**). Various trials were conducted to determine the optimal HRWRA dosage. Once the HRWRA dosage was determined, 50 mm cube specimens were cast, cured under both MC and WB regimens, and tested at seven days to assess the compressive strength of MK-modified UHPC mixtures**.**

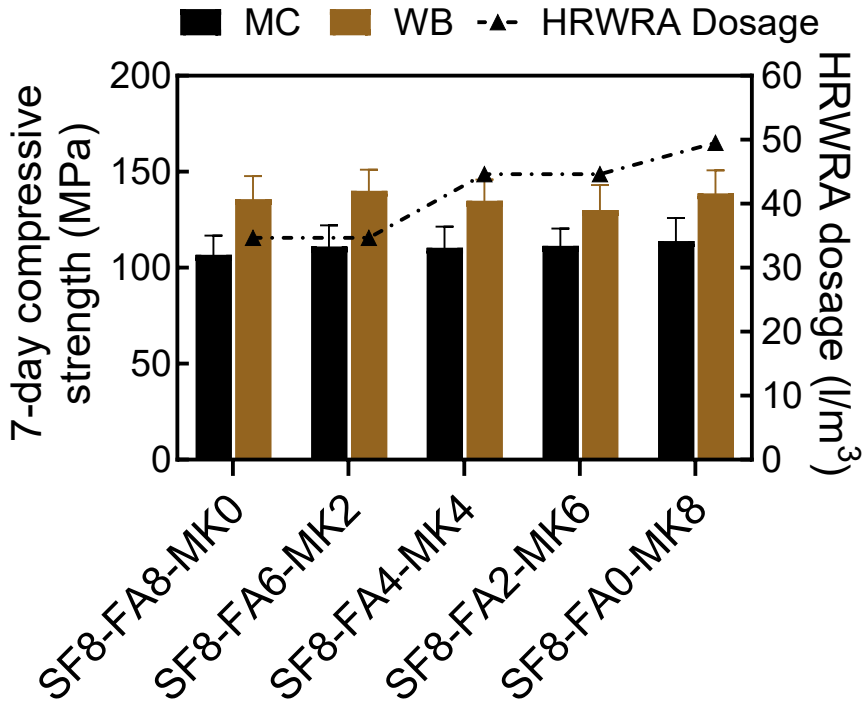

Figure 6. Effect of MK content on HRWRA dosage and seven-day compressive strength of UHPC mixtures.

The results clearly indicated an increase in the dosage of HRWRA as MK dosage increased from 0% to 100%, replacing FA (**Figure 6**) to maintain the required flow. This observation aligns with evidence that incorporating MK reduces concrete workability, likely due to the larger surface area of MK particles compared to FA particles [59, 60]. SEM imaging (**Figure 4**) on raw MK powder reveals that particle shape can influence the water demand of a material. Finer and more irregularly shaped particles, as observed in MK (**Figure 4(c)**), may contribute to a higher water demand compared to the coarser and more spherical particles typically found in FA (**Figure 4(b))** [61].

Furthermore, **Figure 6** illustrates that the seven-day compressive strengths of all the UHPC mixtures cured under MC and WB regimens gradually increased up to 6.75% and 2.2%,

respectively, with the increase in MK content replacing FA. Specimens produced from the UHPC mixture produced with 100% FA replaced with MK (SF8-FA0-MK8), cured under WB regimen demonstrated a compressive strength of 139 MPa. The increase in compressive strength due to higher MK content is likely because MK's finer particles and more reactive surface area enable better packing, improved compaction, reduced porosity, and the formation of additional cementitious phases, enhancing strength development [62, 63, 64].

Based on these preliminary results, mixture SF8-FA0-MK8, which represents a 100% replacement of FA with MK designated as MK modified UHPC, successfully met the required flow and compressive strength properties for UHPC class material. As a result, this mixture has been selected as one of the final mixtures for further testing and development.

3.3.2 Diatomaceous Earth as SCM to replace fly ash

FA was replaced by DE in a similar manner as in the case of MK replacement (section 3.2.1). **Figure 7** illustrates how DE content affects the HRWRA dosage and the seven-day compressive strengths of UHPC mixtures cured under MC and WB conditions. A decrease in the flow was observed as the DE content increased, which resulted in an increase in HRWRA dosage (**Figure 7**). The increased water demand with higher DE content is due to DE's water-absorbing characteristics and porous microstructure, as well as the greater quantity of finer DE particles needing more water to become wet compared to FA particles [65, 66]. As shown in the scanning electron microscopy imaging of DE (**Figure 8)**, its micro components are characterized by a highly dense porous structure resulting from the shells of fossilized diatoms, with submicrometer open pores ranging from 0.3 to 0.8 μm in diameter.

It is also evident from **Figure 7** that the UHPC mixture with 25% replacement level of FA with DE (SF8-FA2-DE6) cured under WB regimen exhibited greatest compressive strength among all the replacement levels while the UHPC mixture with 100% replacement of FA with DE (SF8-FA0-DE8) exhibited a compressive strength 128 MPa when cured under WB regimen. Although SF8-FA0-DE8 did not have the highest compressive strength compared to other mixtures in its group, it met the target workability and compressive strength. Consequently, to achieve the primary research goal of complete FA replacement, SF8-FA0-DE8 was selected for further testing and development as the DE-modified UHPC.

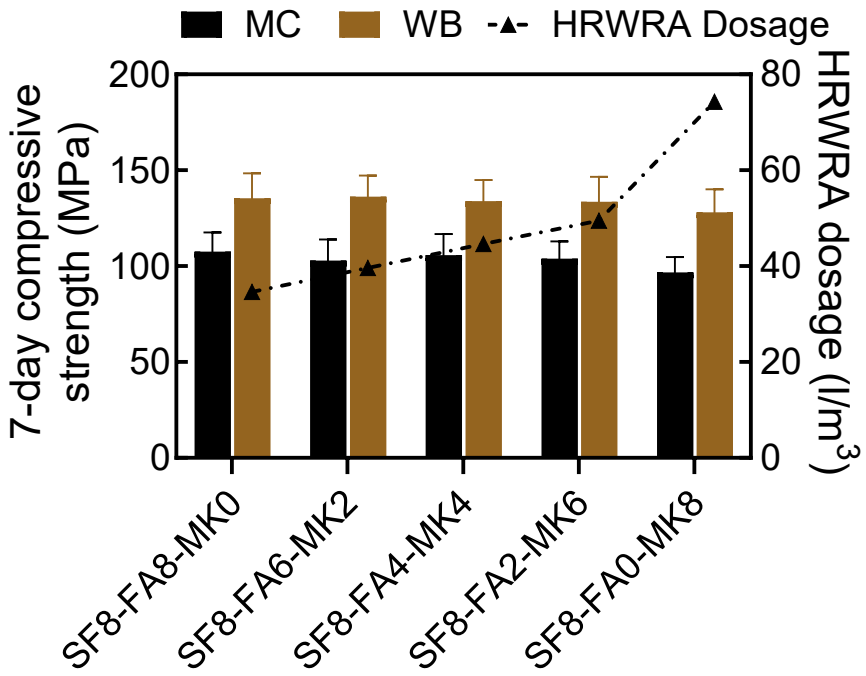

Figure 7. Effect of DE content on HRWRA dosage and seven-day compressive strength of trail UHPC mixtures.

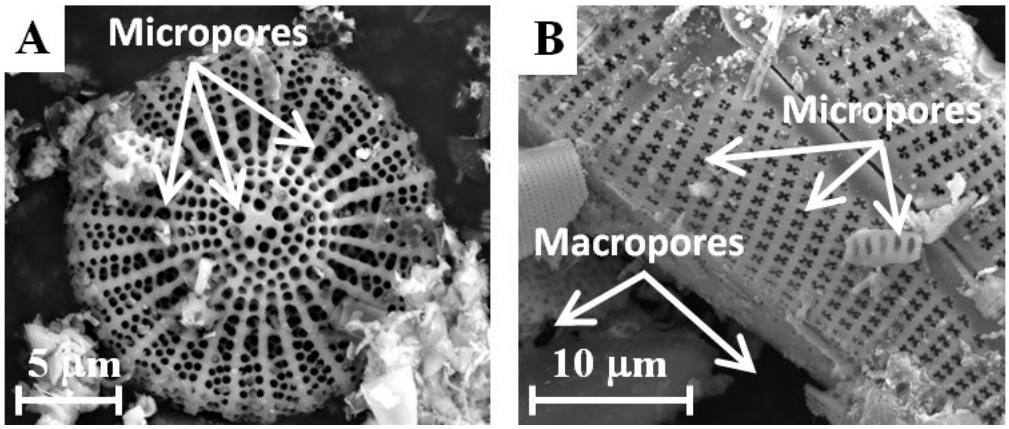

Figure 8. Representative SEM images of DE powder containing different diatoms with microporous structures associated with the intrinsic diatom shell structure and macropores resulting from the granular nature of the powder.

3.3.3. Metakaolin as SCM to replace silica fume in DE modified UHPC mixture

After developing DE modified UHPC by replacing FA with DE, an attempt was made to completely eliminate SF along with FA, as SF is not only expensive but can also cause health issues. MK was used to replace SF in the DE modified UHPC to produce a new MK-DE mixture

formulation (SF0-FA0-MK8-DE8). This formulation exhibited the desired compressive strength and workability. The desired flow of 203 mm to 229 mm was achieved without changing the HRWRA dosage that was used for DE modified UHPC mixture. **Figure 9** compares the compressive strength of MK-DE mixture SF0-FA0-MK8-DE8 with that of the control UHPC mixture (SF8-FA0-MK/DE0) and DE modified UHPC mixture (SF8-FA0-DE8).

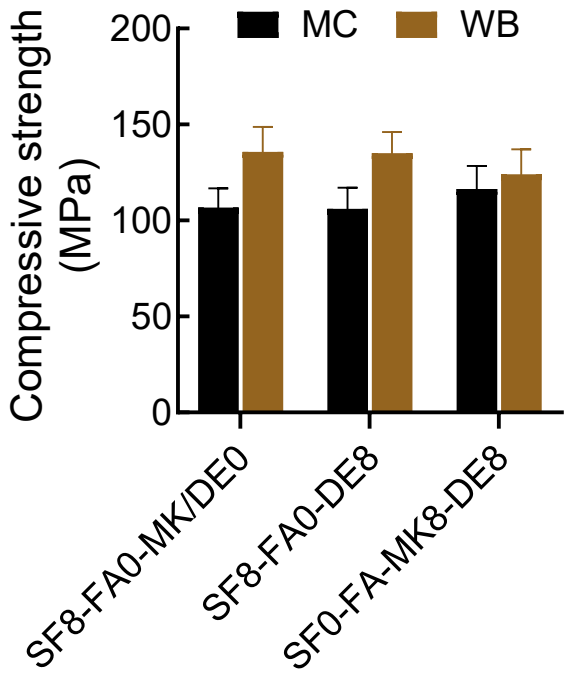

Figure 9. Seven-day compressive strengths of control UHPC, DE-modified UHPC, and MK-DE modified UHPC mixtures cured under both MC and WB curing regimens.

In the MC regimen, the MK-DE mixture exhibited greater compressive strengths than the control mixture and DE modified mixture by 9% and 17.5%, respectively. However, decrease in compressive strength was observed in MK-DE mixture cured under WB curing regimen when compared to control and DE modified mixtures that contain SF by 8.7% and 9.1%, respectively. This decreased compressive strength in MK-DE mixture when cured under WB curing regimen can be traced back to the accelerated strength development of the control UHPC mixture during WB curing. This is facilitated by the highly reactive pozzolanic properties of SF, that are especially effective at elevated temperatures. The increased temperature hastens the hydration process, with SF particles actively engaging in chemical reactions with portlandite and water. This interaction leads to the formation of extra C–S–H gel through secondary reactions, that is instrumental in densifying the cement matrix and, as a result, boosting compressive strength in mixtures containing SF [67, 68, 69, 70]. The absence of SF in MK-DE mixtures could be the reason for lower compressive strength when cured under WB curing regimen.

Based on the results from preliminary investigation as discussed above, four final UHPC mixtures were selected for further investigations: Control, MK-modified UHPC, DE-modified UHPC, and MK-DE-modified UHPC. These formulations were used for further testing, including assessments of compressive strengths up to 56 days, flexural performance, modulus of elasticity, and split tensile strength and were discussed in detail below.

3.4. Compressive strength

3.4.1. Effect of the type of SCM, cured under both MC and WB curing regimens

Average compressive strengths at 3-, 7-, 28-, and 56- days for six 50 mm cubes from each of the four final mixtures cured under both MC and WB regimens are presented in the **Figures 10 and 11**, respectively. In MC curing regimen, the greatest compressive strength of 142 MPa was exhibited by MK modified UHPC mixture at 56-days. However, at 28 days, all the three modified UHPC mixtures (MK, DE, and MK-DE) showed greater compressive strengths than the control mixture by 10%, 5%, and 3.5% respectively. Under WB curing regimen, the greatest compressive strength of 146 MPa was observed in MK modified UHPC mixture at 56 days. Also, at 28 days, MK modified UHPC mixture exhibited marginally greater compressive strength (by 3.6%) than the control UHPC mixture, whereas DE and MK-DE modified UHPC mixtures exhibited lower compressive strengths than to the control mixture by 1.14% and 7.19%, respectively. This suggests that FA can be completely replaced by MK, leading to enhanced compressive strengths. This could partially be due to the size of MK particles (usually under 2 microns), which is significantly smaller than cement particles but larger than the particles of SF [71]. The utilization of MK is known to have a substantial impact on the pore structure and calcium hydroxide content of the hardened cement matrix in concrete, owing to its superior purity and pozzolanic reactivity [72, 73]. While DE modified UHPC led to a slight decrease in compressive strength than control UHPC (by 1.14%; $p > 0.05$), it remains a viable replacement for FA. Additionally, the MK-DE modified UHPC, without SF and FA, yielded comparable results to the control UHPC mixture whose results are consistent with [30].

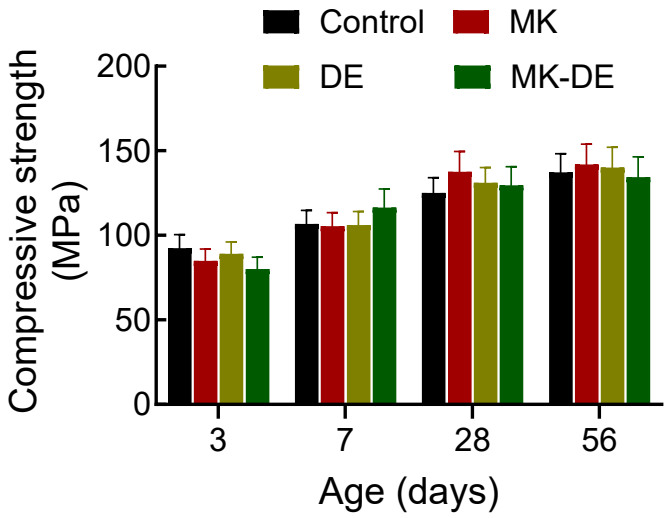

526 **Figure 10**. Compressive strength of MK, DE, and MK-DE- modified UHPC mixtures cured under
527 MC curing regimen.

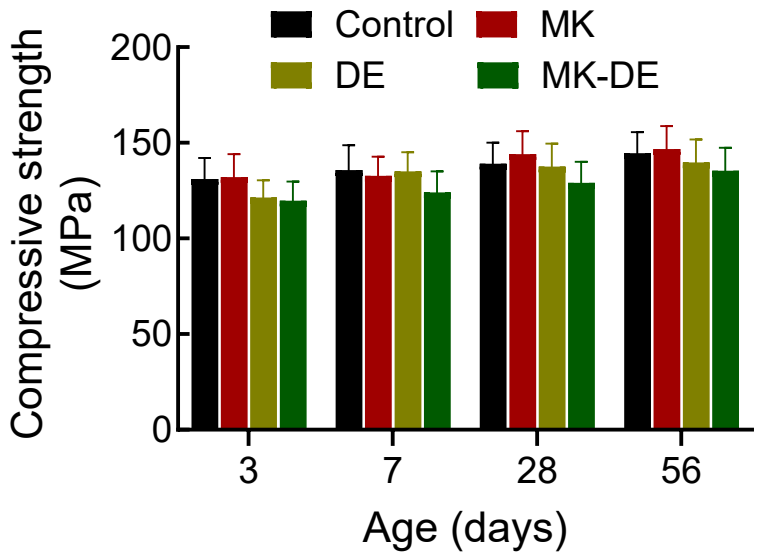

528

529 **Figure 11**. Compressive strength of MK, DE, and MK-DE- modified UHPC mixtures cured under
530 WB curing regimen.

531

532 **3.4.2. Effect of age on compressive strength of UHPC mixtures cured under both MC and**
533 **WB curing regimens**

534 The ratios of compressive strength at 3, 7, and 56 days with respect to 28-day strength are depicted
535 in **Figure 12**. This assumes compressive strength at 28 days is 100% of all the UHPC mixtures
536 cured under both MC and WB curing regimens. The compressive strengths of all the mixtures
537 cured under MC and WB regimens increased with age, but at a reduced rate of increase. The reason
538 was that the reaction rate of cement hydration and the number of hydration products dominated
539 the early strength of concrete mixtures, and were gradually retarded and reduced with increasing
540 time [74].

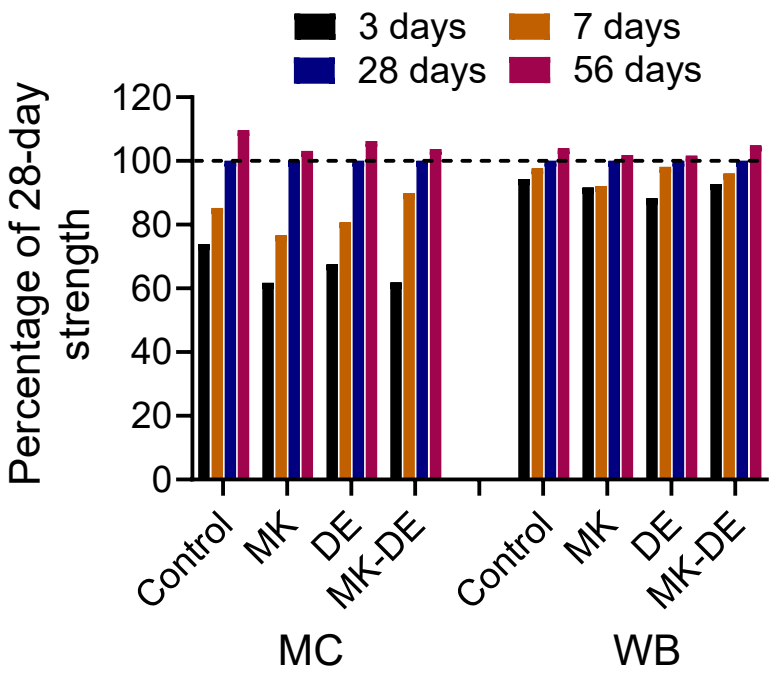

Figure 12. Relative gain of compressive strength with time in MC curing regimen.

When compared to all the mixtures cured under the MC regimen, the control mixture exhibited a remarkable early age compressive strength at three days, achieving 73.9% of its 28-day compressive strength. This was expected because FA reacts more quickly than MK and DE [8, 75]. It can also be observed from **Figure 12** that FA in the control mixture contributes to later age strength gain more than any other UHPC mixture that contain alternative SCM in this study. This is attributed to the fact that, despite the slow pozzolanic reaction, FA can refine the microstructure over the long term [76]. However, MK, DE, MK-DE modified UHPC mixtures showed significant early strength development, reaching approximately 62%, 67%, and 62% of their 28-day compressive strength in three days, respectively. After 28 days, there was a little strength gain (less than 10%) in all the UHPC mixtures.

Under the WB regimen, 90% of the 28-day compressive strength was attained at three days in all the mixtures except in DE modified UHPC mixture. DE modified UHPC mixture exhibited 88% of its 28-day strength at three days. The reason for the greater compressive strengths at three days in these mixtures can be attributed to accelerated hydration reactions and reduction in nanoscale pores compared to specimens cured at ambient temperatures [77, 78, 79] and therefore, more hydration products were available to fill up the micropores. Furthermore, it is interesting to note that the 28-day compressive strength of the specimens produced from control UHPC mixture and cured under WB regimen is only 11.3% greater when compared to the MC cured specimens at 28 days, while all the other three modified UHPC mixtures had only 5% greater strengths in WB when compared to MC.

A one-way ANOVA test was performed to assess the statistical significance of the difference in compressive strengths between specimens cured in MC and WB at the age of 56 days. However, in terms of the 56-day compressive strengths, no statistically significant difference ($p > 0.05$) was noted in compressive strength between the two curing regimens for all UHPC mixtures, except in the case of the MK-modified UHPC mixture. This indicates that MK alleviated the potential adverse effects of elevated temperatures on the properties of UHPC. The incorporation of MK mitigates any detrimental impacts of heat treatment on the microstructure, eliminating any observable interfacial transition zone (ITZ) between the aggregate and the matrix [80]. Hence, based on the SCMs utilized in this research, it can be concluded that MK assists in mitigating concerns such as thermal cracking, ensuring the long-term integrity of the concrete.

The convergence in compressive strengths observed in control, DE- and MK-DE modified UHPCs at later ages between WB and MC regimens highlights a key factor in their similarity. The accelerated hydration facilitated by WB curing at early ages is primarily attributed to elevated temperatures. However, as time progresses, the influence of these heightened temperatures gradually diminishes. By the 56^{th} day, UHPC cured under both WB and MC methods has had ample time to attain comparable strengths, as the temperature-related effects become less pronounced.

This finding suggests that, from a sustainability perspective, the water bath curing regimen may not be essential for longer curing ages. The reduced reliance on elevated temperatures in the later stages of curing implies that more environmentally friendly or energy-efficient curing methods could be explored without compromising the ultimate compressive strength of the UHPC. This not only enhances the sustainability profile of the curing process but also opens avenues for the adoption of practices that align with eco-friendly principles in the production of UHPC mixtures. One of the energy-efficient curing methods could be combined curing, i.e., combination of short term (three days) of WB and MC until the day of testing [81, 82]. This would help in accelerating the pozzolanic reaction and enhanced microstructure of UHPC in the initial days as UHPC contains a high concentration of cementitious materials and fine aggregates, which require thorough hydration to achieve the desired mechanical properties.

3.4.3. Effect of specimen size on compressive strength of UHPC mixtures cured under both MC and WB curing regimens

As the size of the specimen increases, the compressive strength tends to decrease due to the larger volume being more likely to contain an element of low strength [83]. While there is ample research available on the effects of specimen size on the compressive strength of conventional concrete, limited data exists for UHPC mixtures. Therefore, the effect of specimen size on compressive strength of UHPC was investigated in this study.

In this study, compressive strengths of 50 mm and 100 mm cube specimens were compared to study the effect of specimen size on UHPC compressive strength (**Figure 13**). To enable a straightforward comparison, ratios for the compressive strength ratios of 50 mm and 100 mm cubes

from all the UHPC mixtures were computed and presented in **Table 5**. The ratios obtained in this study were in consistent with the literature [84].

Statistical analyses have been conducted to assess the impact of specimen size using one-way ANOVA. The results indicate a statistically significant difference ($p < 0.05$) in the compressive strength of UHPC mixtures between 50 mm and 100 mm cube specimens. This difference holds true irrespective of the SCM used, curing regimen, and the testing age.

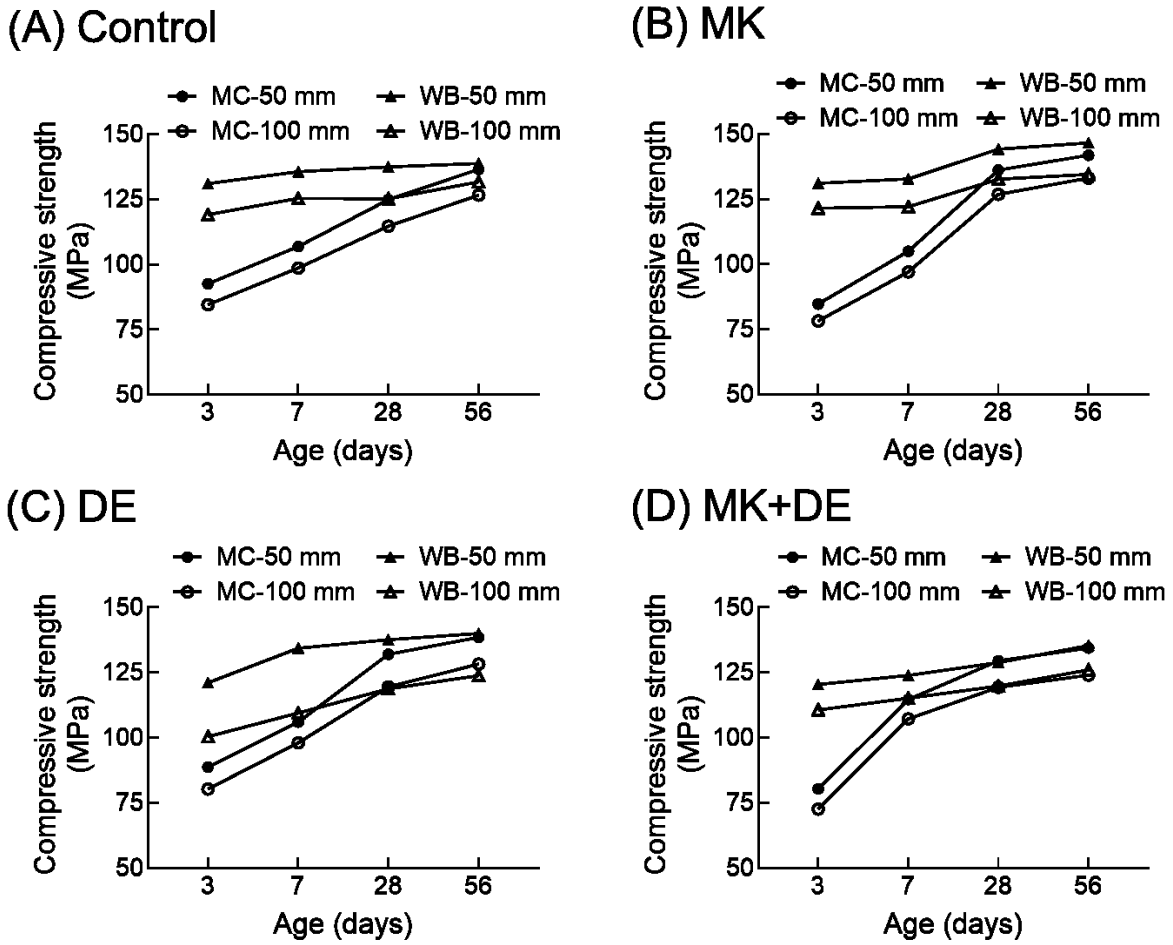

Figure 13. Compressive strength of 50 mm and 100 mm cube specimens cured under MC and WB regimens for 3, 7, 28 and 56 days.

Table 5. Compressive strength ratios of 50 mm to 100 mm cubes, for different UHPC mixtures cured under MC and WB regimens, for 3, 7, 28, and 56 days.

Mixture Designation	3 days		7 days		28 days		56 days	
	MC	WB	MC	WB	MC	WB	MC	WB
Control	1.09	1.10	1.08	1.08	1.09	1.09	1.09	1.10
MK	1.09	1.09	1.09	1.09	1.09	1.09	1.12	1.09
DE	1.11	1.21	1.08	1.24	1.10	1.17	1.09	1.12
MK-DE	1.10	1.08	1.09	1.09	1.09	1.08	1.09	1.09

3.5. Flexural Strength

Flexural tests were conducted on 75 mm × 100 mm × 400 mm prismatic UHPC specimens. From these tests, various response parameters were obtained and analyzed. The load-deflection relationship emerged as a critical metric, offering comprehensive insights into both pre- and post-cracking behaviors of UHPC mixtures incorporating alternative SCMs. The average first peak strength (modulus of rupture- MOR), peak strength, toughness, residual strengths at L/600 (f_{600}^{D}) and L/150 (f_{150}^{D}), and equivalent flexural strength ratios at L/600 ($R_{T,600}^{D}$) and L/150 ($R_{T,150}^{D}$) of all the UHPC mixtures were calculated and presented in **Table 6**.

Table 6. Flexural strength results from 75 mm × 100 mm × 400 mm prismatic UHPC specimens.

Curing Regimen		**MC**					**WB**			
Mixture		**Control**	**MK**	**DE**	**MK-DE**		**Control**	**MK**	**DE**	**MK-DE**
First peak strength (MPa)	7 day	10.1	9.4	8.4	9.3		9.6	9.3	8.3	9.1
	28 day	10.9	9.8	8.9	10.2		10.2	11.7	10.5	11.3
Peak strength (MPa)	7 day	11.7	12.2	10.1	10.3		11.7	13.3	12	12.1
	28 day	12	12.7	11.1	11.6		14.8	14.5	11.8	13
Toughness at 28 days (Joules)	L/600	13	13.8	13	12.4		11.9	14.42	10.7	11.9
	L/150	49.9	49.3	48.6	52.5		46.3	48.4	39.4	38.4
Residual strength at L/150 (MPa)	7 day	5.9	7.7	4.6	7.2		7.4	7.7	4.1	5
	28 day	7	8.7	6.4	7.9		7.6	8	4.5	5.9
Residual strength at L/600 (MPa)	7 day	10.7	11.4	9	11.2		10.2	12.8	8.5	9.9
	28 day	11.4	11.9	11.2	11.8		11.3	14.1	10.3	10.2
Equivalent flexural strength at L/150 (%)	7 day	72.5	71.2	82.1	84.1		75.6	77.5	69.6	79.5
	28 day	81.2	72.8	79.2	86.3		63.4	80.3	66	77.2
Equivalent flexural strength at L/600 (%)	7 day	82.4	83.5	84.7	90.5		83.2	83.4	78.7	88.7
	28 day	85	84.1	83.8	92.6		67.8	86.8	76	82.5

Figure 14 shows the load-deflection curves for all the UHPC mixtures cured under MC and WB curing regimen tested at seven and 28 days. Each load-deflection curve initiates with a steep linear segment, signifying prominent initial stiffness. Following this, the curve demonstrates nonlinearity until encountering the first cracking point, signifying a decline in initial stiffness due to the formation of internal microcracks. At the first cracking point, the load-deflection curve experienced a drop in all the mixtures, with a more pronounced decrease evident in specimens

cured under MC regimen compared to those cured under WB. All the mixtures exhibited a smooth tension stiffening region after the initiation of first crack with a deflection capacity beyond L/150.

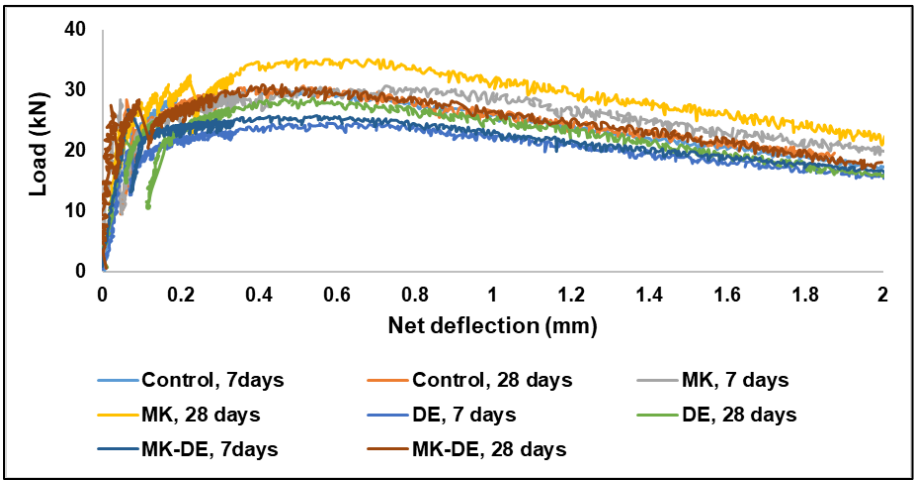

(a)

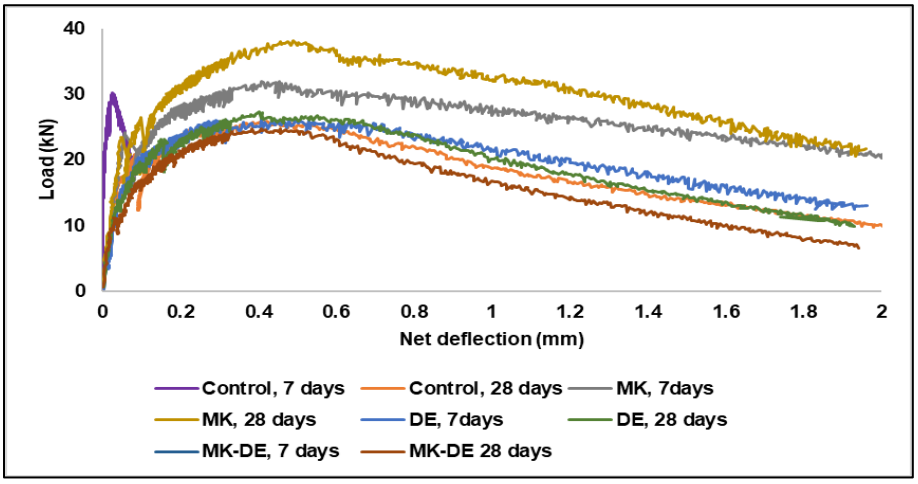

(b)

Figure 14. Load-deflection curves for (a) MC cured specimens at seven and 28 days (b) WB cured specimens at seven and 28 days.

Figure 15 presents the main flexural properties first peak strength (MOR) and peak strength. In terms of MOR values, the control UHPC mixture performed better than the modified UHPC mixtures. The greatest MOR values of 10.13 MPa and 10.92 MPa at seven and 28 days, respectively, were obtained by the control mixture cured under MC regimen. On the other hand, DE modified UHPC exhibited the lowest MOR values under MC curing regimen. DE modified UHPC cured under MC regimen resulted in the reduction of MOR by 17.5% and 14.9% at seven and 28 days, respectively when compared to control UHPC mixture.

All the mixtures cured under both MC and WB curing regimens exhibited greater MOR values at 28 days compared to those at seven days **(Figure 15)**. The WB curing regimen resulted in a decrease in the MOR values at seven days compared to 28 days for all mixtures, with values marginally lower than those cured under the MC regimen. In contrast, at 28 days, when cured under WB, there was a substantial increase in the MOR values in all the mixtures except the control mixture. MOR values of MK, DE, and MK-DE modified mixtures were 17.65%, 16.75%, and 9.61% greater when compared to those cured under MC regimen. The initial decrease in MOR values at 7 days under WB curing compared to MC regimen may be attributed to slower hydration rates and potential drying of samples, while the subsequent increase in MOR values at 28 days under WB curing suggests enhanced microstructure strengthening through prolonged hydration [85, 86]. However, the control mixture exhibited marginally lower MOR value at 28 days in WB curing compared to MC regimen. This can be attributed to slower pozzolanic reactivity and less efficient hydration kinetics inherent to FA [87], whereas the greater MOR values exhibited by UHPC mixtures containing MK or DE in WB curing might be the result of their higher pozzolanic reactivity and finer particle sizes, which facilitate enhanced flexural strength [30, 65].

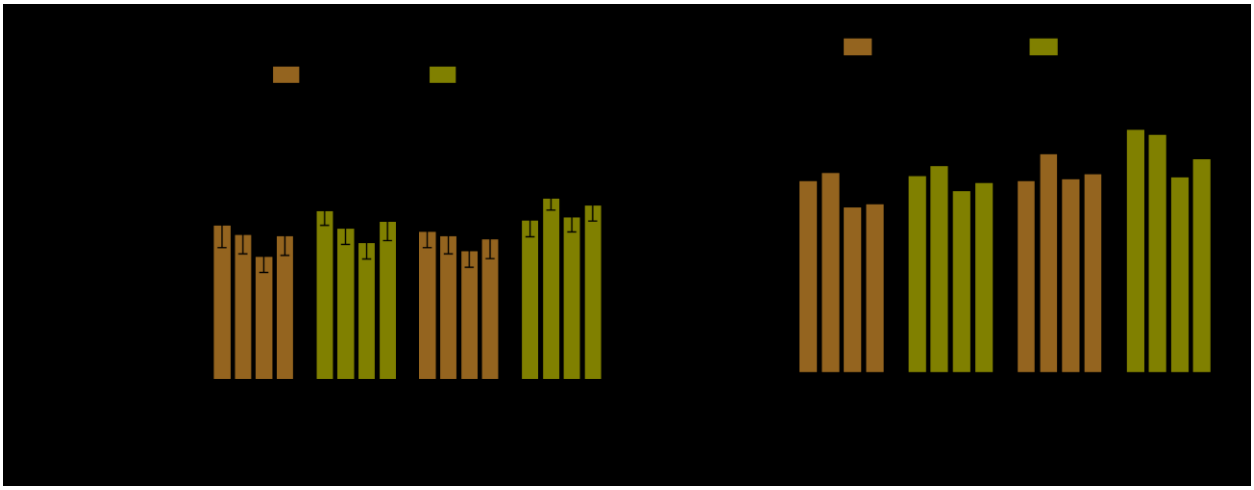

Figure 15. Comparison of seven and 28-day (a) first peak strength (MOR) and (b) peak strengths of control, MK, DE, and MK-DE modified UHPC mixtures cured under MC and WB regimens.

This significant improvement in MOR values can be attributed to the enhanced microstructure of the UHPC mixture resulting from the hydration of both MK and DE at later ages. The peak strengths at seven and 28 days of all four UHPC mixtures cured under MC and WB regimens were depicted in **Figure 15 (b**). All the WB cured UHPC specimens had greater peak strengths than the MC cured specimens. The greatest peak strength of 14.8 MPa was exhibited by control UHPC mixture at 28 days when cured under WB curing regimen followed by MK modified UHPC. DE modified UHPC exhibited the lowest peak strengths when compared to control UHPC mixture by 14.9% and 8% at seven and 28 days respectively under MC curing regimen.

The residual strengths at deflections L/600 (f_{600}^{D}) and L/150, deflections (f_{150}^{D}) were depicted in **Figure 16**. Among all the mixtures, MK modified UHPC cured under WB regimen for 28 days

exhibited greatest residual strengths of 14 MPa and 8 MPa at L/600 and L/150 deflections, respectively, with DE modified UHPC being the least. As in the case of MOR, there is no improvement in residual strengths of control mixture when cured under WB. Similarly, the WB cured UHPC mixtures containing DE displayed residual strengths lower than those of the MC cured DE modified UHPC at seven and 28 days. This trend suggests that the presence of DE does not contribute positively in terms of residual strengths.

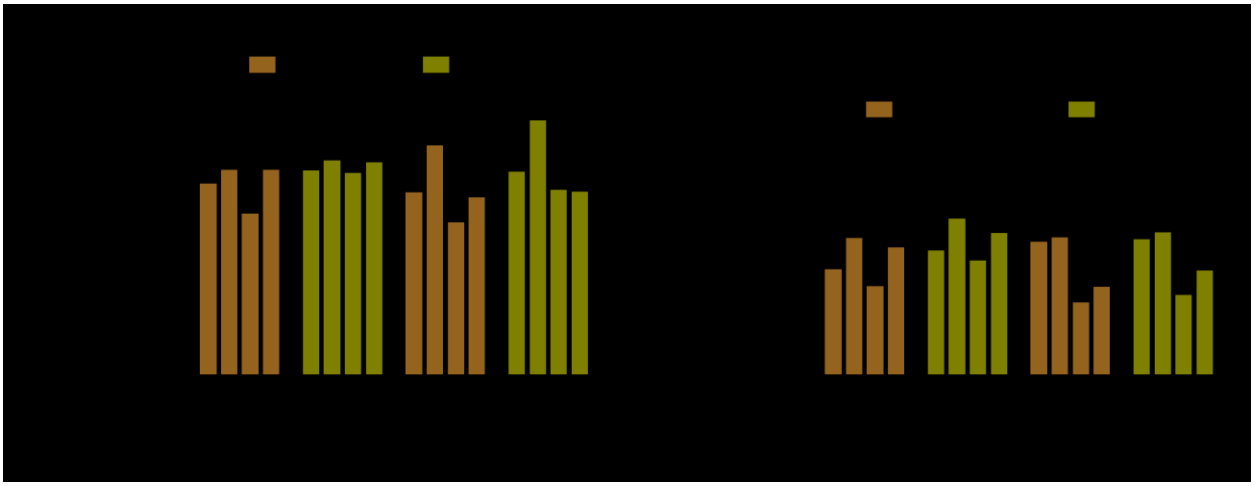

Figure 16. Residual flexural strength (a) at L/600 deflection; and (b) at L/150 deflection.

3.6. Toughness

To properly understand the energy absorption capacity of UHPC mixtures produced with different SCMs and cured under MC and WB curing regimens, toughness values were calculated for all the developed mixtures at deflections L/600 and L/150 and are presented in **Figure 17**. At L/600 deflection, MK modified UHPC showed better performance than the control UHPC mixture by 6% and 14.4% in MC and WB curing regimens, respectively, while, MK-DE modified UHPC had the least toughness values at L/600. However, at deflection of L/150, the MK-DE modified UHPC mixture, cured under MC regimen, exhibited the greatest toughness value of 52.5 Joules at 28 days, which is 5% greater than that of the control UHPC mixture. Both MK and DE modified UHPC mixtures showed toughness values similar to the control UHPC mixtures at 28 days cured under MC curing regimen, with decreases of 1.2% and 2.6%, respectively. Whereas, in the WB curing regimen, at 28 days, MK-DE modified UHPC mixtures exhibited the lowest toughness value, with the DE modified UHPC mixture following closely. This suggests that DE has a negative effect on toughness when cured under WB conditions.

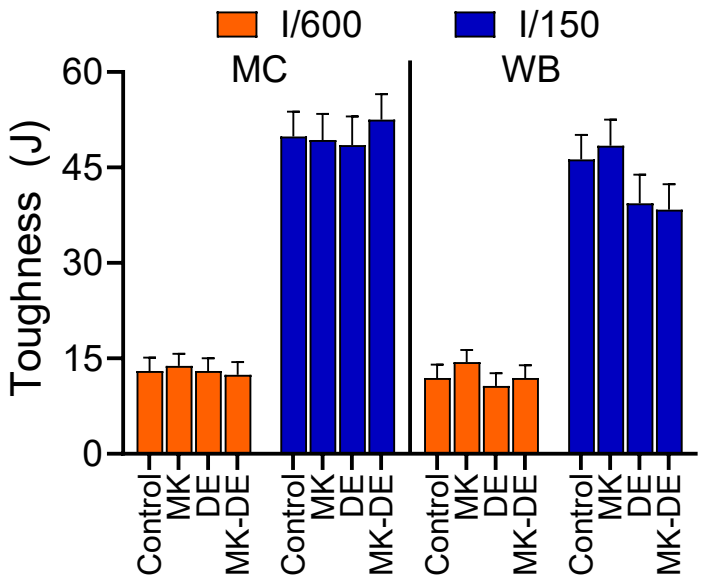

Figure 17. Toughness of UHPC mixtures at 28 days measured at L/600 and L/150 deflections.

3.7. Equivalent flexural strength ratios

Equivalent flexural strength ratios ($R^D_{T,n}$) were calculated in accordance with ASTM 1609 [48] to further characterizing the flexural performance of UHPC mixtures containing alternative SCMs:

$$R^D_{T,n} = \frac{nT^D_n}{f_p b d^2}.100\%$$

where, n = deflection ratio corresponding to the toughness measured (e.g., 150 at the deflection of L/150), T^D_n = toughness measured at deflection of L/n, f_p is the peak strength, and b and d are the cross-sectional dimensions of the prismatic specimen.

The ratio obtained offers a standardized measure of the relative flexural strength retained post-cracking at a specified deflection level. For instance, for control UHPC mixture, cured for 28 days under MC curing regimen, the $R^D_{T,150}$ value is 81.2%. This indicates that 81.2% of the peak strength was still present at the deflection corresponding to L/150 deflection. **Figure 18(a)** and **Figure 18(b)** depicts the equivalent flexural strength ratios calculated at deflections corresponding to L/600 and L/150, respectively, for all the mixtures cured under MC and WB regimens. The $R^D_{T,600}$ and $R^D_{T,150}$ ratios are the highest for MC cured MK-DE modified UHPC mixture at 28 days, and the lowest for WB cured control UHPC mixture at 28 days. MK-DE modified UHPC mixture performed better than the control UHPC mixture in both the curing regimens, at both seven and 28 days at both the deflections except in the case of WB cured MK- modified UHPC at 28days. Moreover, at 28 days, MK modified UHPC cured under WB cuing regimen showed better performance than any other UHPC mixtures while DE modified UHPC mixture had the least equivalent flexural strength ratios. This trend persisted even at seven days, where the DE modified

UHPC mixture exhibited lower values than any other UHPC mixtures. These results suggest that WB curing has a detrimental effect on the flexural strength of DE modified UHPC.

Figure 18. Equivalent flexural strengths (a) at L/600 deflection, and (b) at L/150 deflection.

3.8. Splitting tensile strength and modulus of elasticity of UHPC mixtures

100 mm × 200 mm cylindrical specimens for all the four UHPC mixtures, cured under MC curing regimen, were tested at 28 days to evaluate their splitting tensile strength (**Table 7**)**.** The control UHPC mixture exhibited the greatest splitting tensile strength of 9.92 MPa. However, the MK modified UHPC mixture showed a decrease of 8.31% when compared to the control UHPC mixture ($p < 0.05$). Similar finding was reported by Ahmed et.al [60], that the addition of MK reduced the splitting tensile strength of the modified UHPC. This reduction can be attributed to the low w/cm ratio and the low specific surface area of MK, which are known to affect the split tensile strength negatively [88] . Furthermore, the split tensile strength of the DE modified UHPC decreased by 16.5% compared to the control mixture. This reduction in tensile strength is linked to the concrete's lower workability, which can result in a less compact UHPC mixture, ultimately leading to lower tensile strength [38]. In contrast, this decrease was only 8.7% in MK-DE modified UHPC mixture when compared to control mixture.

Table 7 displays the average Poisson ratio and modulus of elasticity values for the UHPC mixtures developed in this study following 28 days of moist curing. Among these, the control UHPC exhibited the greatest modulus of elasticity value of 36,542 MPa with a Poisson's ratio of 0.22. MK-DE mixture exhibited modulus of elasticity and Poisson's values similar to those of control mixture. In contrast, the DE modified UHPC exhibited a relatively lower modulus of elasticity (33,784 MPa), demonstrating a reduction of 8% compared to the control mixture.

Table 7. Effect of split tensile strength, Poisson ratio, and modulus of elasticity of UHPC mixtures.

Mixture	Split tensile strength (MPa)	Poisson's ratio	Modulus of Elasticity (MPa)
Control	9.93	0.22	36,542
MK	9.14	0.21	35,853
DE	8.41	0.20	33,784
MK-DE	9.10	0.21	35,853

3.9. Innovation and limitations

This study presents a significant advancement in the development of sustainable and non-proprietary UHPC by replacing traditional SCMs such as SF and FA with MK and DE. The innovative aspect lies in the successful complete replacement of FA with MK or DE and the combined replacement of both SF and FA using MK and DE. This approach addresses key challenges, including the high cost of SF and the declining availability of FA, while improving the environmental footprint of UHPC. The results demonstrate that MK and DE can maintain comparable mechanical properties to control mixtures, with MK proving particularly effective in enhancing long-term compressive strength under different curing conditions.

However, the research also revealed certain limitations. For example, while the MK-DE modified UHPC exhibited promising compressive strength, the DE-modified mixtures experienced reductions in toughness and splitting tensile strength, highlighting that DE may not perform as well as MK in terms of energy absorption and tensile performance. Additionally, the need for increased dosages of HRWRA to maintain flowability in MK and DE-modified mixtures may present practical challenges in large-scale applications. Furthermore, while WB curing accelerated early-age strength development, its long-term benefits diminished over time, raising questions about its necessity for sustainable construction practices. Despite these limitations, the study underscores the potential of MK and DE to serve as cost-effective, eco-friendly SCMs in UHPC formulations, paving the way for further optimization and investigation into their full potential in various construction applications.

4. Conclusions

This study explores the potential of MK and DE as sustainable and cost-effective alternatives to SF and FA in UHPC. The key findings are summarized below:

Objective Achievement: The complete replacement of FA with MK or DE and the combined replacement of both SF and FA using MK-DE mixtures were successfully achieved, addressing the challenges of high SF costs and declining FA availability.

Material Characterization: Thermogravimetric analysis indicated that MK, with its high thermal stability and pozzolanic reactivity, is a promising alternative to SF, while DE, with its high silica content, offers potential as a sustainable FA substitute.

Rheological and Mechanical Performance: Rheological analysis revealed that MK and DE increased the apparent viscosity of UHPC mixtures while reducing yield stress, suggesting altered flow characteristics. Despite this, the modified mixtures maintained compatibility with standard rheological models. MK-DE mixtures exhibited enhanced compressive strength under moist curing conditions, achieving values similar to or exceeding the control mixture at 28 and 56 days. Flexural and tensile properties varied, with MK-modified mixtures generally outperforming DE-modified ones in toughness and modulus of rupture (MOR).

Sustainability Implications: The use of MK and DE reduced reliance on conventional SCMs, contributing to cost reduction and environmental sustainability. Increased HRWRA dosages were required for these mixtures to maintain workability.

Curing Effects: While warm bath curing accelerated early-age strength development, its benefits diminished over time. Moist curing provided comparable long-term strength, suggesting potential for more energy-efficient curing methods. Warm bath curing is not required unless early-age strength is a priority.

This study introduces a non-proprietary approach to UHPC design using MK and DE, paving the way for more sustainable and economical construction materials. Future studies should explore optimizing these formulations to further enhance mechanical performance and durability.

CRediT authorship contribution statement

Meghana Yeluri: Investigation, Data Curation, Validation, Formal Analysis, Visualization, Writing – Original draft. **Elif G. Ertugral:** Investigation, Data curation, Visualization. **Yashovardhan Sharma:** Writing – Review and Editing. **Chandrasekhar R. Kothapalli:** Methodology, Formal Analysis, Visualization, Supervision, Writing – Review and Editing. **Petru S. Fodor:** Methodology, Writing – Review and Editing. **Srinivas Allena:** Conceptualization, Methodology, Formal Analysis, Resources, Writing – Review and Editing, Supervision, Project Administration.

Declaration of Competing Interest

The authors declare that they have no known competing financial interests or personal relationships that could have appeared to influence the work reported in this paper.

Acknowledgements

The SEM facility used in this work was partially supported by the National Science Foundation (NSF) under Grant No. 1126126. Any opinions, findings, and conclusions or recommendations expressed in this material are those of the authors and do not necessarily reflect the views of the NSF. The authors are thankful to Mr. Miroslav Bogdanovski for the assistance provided with the SEM imaging.

828 References
829

[1] N. Roux, C. Andrade and M. Sanjuan, "Experimental study of durability of reactive powder concretes," *Journal of materials in civil engineering,* vol. 8, no. 1, pp. 1--6, 1996.

[2] O. Bonneau, M. Lachemi, E. Dallaire, J. Dugat and P. Aitcin, "Mechanical properties and durability of two industrial reactive powder concretes," *Materials Journal,* vol. 94, pp. 286--290, 1997.

[3] N. Soliman and A. Tagnit-Hamou, "Study of rheological and mechanical performance of ultra-high-performance glass concrete," *Fibre Reinforced Concrete: from Design to Structural Applications,* vol. 17, 2015.

[4] P. Richard and M. Cheyrezy, "Composition of reactive powder concretes," *Cement and concrete research,* vol. 25, pp. 1501--1511, 1995.

[5] J. Dugat, N. Roux and G. Bernier, "Mechanical properties of reactive powder concretes," *Materials and structures,* vol. 29, no. 4, pp. 233--240, 1996.

[6] M. Schmidt and E. Fehling, "Ultra-high-performance concrete: research, development and application in Europe," *ACI Spec. Publ,* vol. 228, no. 1, pp. 51--78, 2005.

[7] T. Klemens, "Flexible concrete offers new solutions," *Concr. Constr,* vol. 49, p. 72, 2004.

[8] S. Mousavinezhad, G. Gonzales, W. Toledo, J. Garcia, C. Newtson and S. Allena, "A Comprehensive Study on Non-Proprietary Ultra-High-Performance Concrete Containing Supplementary Cementitious Materials," *Materials,* vol. 16, p. 2622, 2023.

[9] V. Van and H. Ludwig, "Proportioning optimization of UHPC containing rice husk ash and ground granulated blast-furnace slag," in *Proceedings of the 3rd International Symposium on UHPC and Nanotechnology for High Performance Construction Materials, Kassel, Germany*, 2012, pp. 197--205.

[10] C. Schr{\"o}fl, M. Gruber and J. Plank, "Preferential adsorption of polycarboxylate superplasticizers on cement and silica fume in ultra-high performance concrete (UHPC)," *Cement and Concrete Research,* vol. 42, no. 11, pp. 1401--1408, 2012.

[11] W. Liao, X. Sun, A. Kumar, H. Sun and H. Ma, "Hydration of binary portland cement blends containing silica fume: A decoupling method to estimate degrees of hydration and pozzolanic reaction," *Frontiers in Materials,* vol. 6, p. 78, 2019.

[12] R. Yu, P. Spiesz and H. Brouwers, "Mix design and properties assessment of ultra-high performance fibre reinforced concrete," *Cement and concrete research,* vol. 56, pp. 29--39, 2014.

[13] C. Taylor, K. Montoya, D. Jauregui, C. Newtson and B. Weldon, "Feasibility analysis of using UHPC in prestressed bridge girders," in *Structures Congress* , 2011, pp. 203--214.

[14] R. Merget, T. Bauer, H. Kupper, S. Philippou, H. Bauer, R. Breitstadt and T. Bruening, "Health hazards due to the inhalation of amorphous silica," *Archives of toxicology,* vol. 75, pp. 625--634, 2002.

[15] H. Zhang, T. Ji, B. He and L. He, "Performance of ultra-high performance concrete (UHPC) with cement partially replaced by ground granite powder (GGP) under different curing conditions," *Construction and Building Materials,* vol. 213, pp. 469--482, 2019.

[16] J. Ma and H. Schneider, "Properties of ultra-high-performance concrete," *Leipzig Annual Civil Engineering Report (LACER),* vol. 7, pp. 25--32, 2002.

[17] M. Soutsos, S. Millard and K. Karaiskos, "Mix design, mechanical properties, and impact resistance of reactive powder concrete (RPC)," in *International workshop on high performance fibre-reinforced cementitious composites in structural applications*, 2005, pp. 549--560.

[18] H. Yazici, "The effect of curing conditions on compressive strength of ultra high strength concrete with high volume mineral admixtures," *Building and environment,* vol. 42, no. 5, pp. 2083--2089, 2007.

[19] Z. Li, "Drying shrinkage prediction of paste containing meta-kaolin and ultrafine fly ash for developing ultra-high performance concrete," *Materials Today Communications,* pp. 74--80, 2016.

[20] N. Van Tuan, G. Ye, K. Van Breugel, A. Fraaij and D. Dai Bui, "The study of using rice husk ash to produce ultra high performance concrete," *Construction and Building Materials,* vol. 25, pp. 2030--2035, 2011.

[21] Z. Wu, C. Shi and W. He, "Comparative study on flexural properties of ultra-high performance concrete with supplementary cementitious materials under different curing regimes," *Construction and Building Materials,* vol. 136, pp. 307--313, 2017.

[22] S. Ahmad, I. Hakeem and M. Maslehuddin, "Development of UHPC mixtures utilizing natural and industrial waste materials as partial replacements of silica fume and sand," *The Scientific World Journal,* 2014.

[23] A. Alsalman, C. Dang and M. Hale, "Development of ultra-high performance concrete with locally available materials," *Construction and Building Materials,* vol. 133, pp. 135--145, 2017.

[24] "ACAA(Americal Coal Ash Association," [Online]. Available: https://acaa-usa.org. [Accessed 23 9 23].

[25] I. Diaz-Loya, M. Juenger, S. Seraj and R. Minkara, "Extending supplementary cementitious material resources: Reclaimed and remediated fly ash and natural pozzolans".

[26] J. Khatib, O. Baalbaki and A. ElKordi, "Metakaolin," in *Waste and supplementary cementitious materials in concrete*, Elsevier, 2018, pp. 493--511.

[27] S. Elavarasan, A. Priya, N. Ajai, S. Akash, T. Annie and G. Bhuvana, "Experimental study on partial replacement of cement by metakaolin and GGBS," *Materials Today: Proceedings,* vol. 37, pp. 3527--3530, 2021.

[28] "Calorimetric study of alkaline activation of calcium hydroxide--metakaolin solid mixtures," *Cement and Concrete Research,* vol. 31, no. 1, pp. 25--30, 2001.

[29] K. Weise, N. Ukrainczyk and E. Koenders, "Pozzolanic Reactions of Metakaolin with Calcium Hydroxide: Review on Hydrate Phase Formations and Effect of Alkali Hydroxides, Carbonates and Sulfates," *{Materials & Design,* p. 112062, 2023.

[30] A. Tafraoui, G. Escadeillas, S. Lebaili and T. Vidal, "Metakaolin in the formulation of UHPC," *Construction and Building Materials,* vol. 23, no. 2, pp. 669--674, 2009.

[31] E. Kadri, S. Kenai, K. Ezziane, R. Siddique and G. De Schutter, "Influence of metakaolin and silica fume on the heat of hydration and compressive strength development of mortar," *Applied Clay Science,* vol. 53, no. 4, pp. 704--708, 2011.

[32] A. {Mardani-Aghabaglou, G. Sezer and K. Ramyar, "Comparison of fly ash, silica fume and metakaolin from mechanical properties and durability performance of mortar mixtures view point," *Construction and Building Materials,* vol. 70, pp. 17--25, 2014.

[33] D. Pillay, O. Olalusi, M. Kiliswa, P. Awoyera, J. Kolawole and A. Babafemi, "Engineering performance of metakaolin based concrete," *Cleaner Engineering and Technology,* vol. 6, p. 100383, 2022.

[34] S. Tongbo, W. Bin, Z. Lijun and C. Zhifeng, "Calcined Clays for Sustainable Concrete: Proceedings of the 1st International Conference on Calcined Clays for Sustainable Concrete," in *Springer*, 2015.

[35] S. Zheng, Z. Sun, Z. Hu and G. Zhang, "The processing and utilization of China diatomite resource and its development trend," *Earth Science Frontiers,* vol. 21, no. 5, pp. 274-280, 2014.

[36] S. Ash, "Mineral commodity summaries 2019," US Geological Survey, Reston, VA, 2019.

[37] S. Kou, C. Poon and M. Etxeberria, "Influence of recycled aggregates on long term mechanical properties and pore size distribution of concrete," *Cement and Concrete Composites,* vol. 33, no. 2, pp. 286-291, 2011.

[38] M. Hasan, T. Saidi, A. Mubarak and M. Jamil, "Effect of calcined diatomaceous earth, polypropylene fiber, and glass fiber on the mechanical properties of ultra-high-performance fiber-reinforced concrete," *Journal of the Mechanical Behavior of Materials,* vol. 32, p. 20220275, 2023.

[39] M. Hasan, A. Riski, T. Saidi, H. Husaini and P. Rahman, "Flexural and splitting tensile strength of high strength concrete with diatomite micro particles as mineral additive," in *In Defect and Diffusion Forum*, Trans Tech Publications Ltd, 2020, pp. 50-55.

[40] A. Tangit-Hamou, N. Petrov and K. Luke, " Properties of concrete containing diatomaceous earth," *ACI Materials Journal,* vol. 100, no. 1, pp. 73-78, 2003.

[41] W. Du, "Study on preparation of ultra-high strength and high performance concrete from diatomite and its mechanical properties," in *In IOP Conference Series: Earth and Environmental Science*, IOP Publishing, 2019, p. 012054.

[42] N. Degirmenci and A. Yilmaz, "Use of diatomite as partial replacement for Portland cement in cement mortars.," *Construction and Building Materials,* vol. 23, no. 1, pp. 284-288, 2009.

[43] "ASTM C33: Standard specification for concrete aggregates," ASTM International , West Conshohocken, PA, 2018.

[44] "ASTM C128: Standard Test Method for Relative Density (Specific Gravity) and Absorption of Fine Aggregate," ASTM International, West Conshohocken, PA, 2015.

[45] "ASTM C1856:Standard practice for fabricating and testing specimens of Ultra-high performance concrete," ASTM International, West Conshohocken, PA, 2017.

[46] "ASTM C1437-20, Standard Test Method for Flow of Hydraulic Cement Mortar, West Conshohocken, PA," *ASTM International,* 2020, DOI: 10.1520/C1437-20.

[47] "Standard Test Method for Compressive Strength of Hydraulic Cement Mortars (Using 2-in. or [50-mm] Cube Specimens)," ASTM International, West Conshohocken, PA, 2020.

[48] "ASTM C1609: Standard Test Method for Flexural Performance of Fiber-Reinforced Concrete (Using Beam With Third-Point Loading)," ASTlM International, West Conshohocken, PA, 2019.

[49] "Standard Test Method for Splitting Tensile Strength of Cylindrical Concrete Specimens," ASTM International, West Conshohocken, PA, 2017.

[50] "Standard Test Method for Static Modulus of Elasticity and Poisson's Ratio of Concrete in Compression," ASTM International, West Conshohocken, PA, 2017.

[51] T.-Y. Shin and J. Kim, "First step in modeling the flow table test to characterize the rheology of normally vibrated concrete," *Cement and Concrete Research,* vol. 152, p. 106678, 2022.

[52] Y. Song, J. Xiang, W. Cui and G. Xiong, "Anhydrous ethanol as a medium used to grind soda-lime glass for cement-based materials preparation: Evaluating its rheological behavior by the Herschel--Bulkley and Modified--Bingham models," *Journal of Building Engineering,* vol. 63, p. 105553, 2023.

[53] R. Campos and G. Maciel, "Test protocol and rheological model influence on determining the rheological properties of cement pastes," *Journal of Building Engineering,* vol. 44, p. 103206, 2021.

[54] Y. Xu, Y. Yu, P. Li, M. Liu, L. Zhu, H. Zhang, C. Zhang, G. Hu, M. Hu and J. Guo, "Rheological behavior of oil well cement pastes containing various types of dispersants at different hydration temperatures," *Colloids and Surfaces A: Physicochemical and Engineering Aspects,* vol. 624, p. 126821, 2021.

[55] Y. Peng, K. Ma, C. Unluer, W. Li, S. Li, J. Shi and G. Long, "Method for calculating dynamic yield stress of fresh cement pastes using a coaxial cylinder system," *Journal of the American Ceramic Society,* vol. 104, no. 11, pp. 5557--5570, 2021.

[56] A. Habib, I. Aiad, F. El-Hosiny and A. Mohsen, "Studying the impact of admixtures chemical structure on the rheological properties of silica-fume blended cement pastes using various rheological models," *Ain Shams Engineering Journal,* vol. 12, no. 2, pp. 1583--1594, 2021.

[57] D. Feys, R. Verhoeven and G. De Schutter, "Fresh self compacting concrete, a shear thickening material," *Cement and Concrete Research,* vol. 38, no. 7, pp. 920--929, 2008.

[58] A. Papo and L. Piani, "Flow behavior of fresh Portland cement pastes," *Particulate science and technology,* vol. 22, no. 2, p. 2004, 201--212.

[59] U. Biswal and P. Dinakar, "Influence of metakaolin and silica fume on the mechanical and durability performance of high-strength concrete made with 100\% coarse recycled aggregate," *Journal of Hazardous, Toxic, and Radioactive Waste,* vol. 26, no. 2, p. 04022004, 2022.

[60] J. Ahmad, A. Majdi, M. Arbili, A. Deifall and M. Naqash, "Mechanical, Durability and Microstructure Analysis Overview of Concrete Made with Metakaolin (MTK)," *Buildings,* vol. 12, p. 1401, 2022.

[61] T. Singh, R. Siddique and S. Sharma, "Effectiveness of using Metakaolin and fly ash as supplementary cementitious materials in pervious concrete," *European Journal of Environmental and Civil Engineering,* vol. 26, no. 15, pp. 7359--7382, 2022.

[62] S. Barbhuiya, P. Chow and S. Memon, "Microstructure, hydration and nanomechanical properties of concrete containing metakaolin," *Construction and Building Materials,* vol. 95, pp. 696--702, 2015.

[63] W. Ding, Y. He, L. Lu, F. Wang and S. Hu, "Mechanical property and microstructure of quaternary phase paste blended with metakaolin," *Cement and Concrete Composites,* vol. 118, p. 103934, 2021.

[64] W. Long, J. Liu and C. He, "A facile approach to disperse metakaolin for promoting compressive strength of cement composites," *Construction and Building Materials,* vol. 404, p. 133268, 2023.

[65] M. Hasan, M. Jamil and T. Saidi, "Mechanical properties and durability of ultra-high-performance concrete with calcined diatomaceous earth as cement replacement," *Journal of the Mechanical Behavior of Materials,* vol. 32, p. 20220272, 2023.

[66] D. Kastis, G. Kakali, S. Tsivilis and M. Stamatakis, "Properties and hydration of blended cements with calcareous diatomite," *Cement and concrete research,* vol. 36, pp. 1821--1826, 2006.

[67] R. Zhong, K. Wille and R. Viegas, "Material efficiency in the design of UHPC paste from a life cycle point of view," *Construction and Building Materials,* vol. 160, pp. 505--513, 2018.

[68] S. Abdal, W. Mansour, N. Ibrahim, A. Mohammed, O. Aref, . A. Yasin and h. Mahmoud, "Application of Ultra-High-Performance Concrete in Bridge Engineering: Current Status, Limitations, Challenges, and Future Prospects," *Buildings,* vol. 13, no. 1, p. 185, 2023.

[69] P. J. Monteiro, S. A. Miller and A. Horvath, "Towards sustainable concrete".

[70] P. LI, H. Brouwers, W. Chen and Q. Yu, "Optimization and characterization of high-volume limestone powder in sustainable ultra-high performance concrete," *Construction and Building Materials,* vol. 242, p. 118112, 2020.

[71] J. Ding and Z. Li, "Effects of metakaolin and silica fume on properties of concrete," *Materials Journal,* vol. 99, pp. 393--398, 2002.

[72] J. Ambroise, S. Martin-Calle and J. Pera, "Pozzolanic behavior of thermally activated kaolin," *Special Publication,* vol. 132, pp. 731--748, 1992.

[73] J. Kostuch, G. Walters and T. Jones, "High performance concretes incorporating metakaolin: a review," *Concrete,* vol. 2, pp. 1799--811, 2000.

[74] R. Shao, C. Wu, J. Li, Z. Liu, P. Wu and Y. Yang, "Mechanical behaviour and environmental benefit of eco-friendly steel fibre-reinforced dry UHPC incorporating high-

volume fly ash and crumb rubber," *Journal of Building Engineering,* vol. 65, p. 105747, 2023.

[75] P. Rangaraju and Z. Li, "Development of UHPC using ternary blends of ultra-fine class F fly ash, meta-kaolin and portland cement," in *International Interactive Symposium on Ultra-High Performance Concrete*, Iowa State University, 2016.

[76] Z. Rong, W. Sun, H. Xiao and W. Wang, "Effect of silica fume and fly ash on hydration and microstructure evolution of cement based composites at low water--binder ratios," *Construction and Building Materials,* vol. 51, pp. 446--450, 2014.

[77] D. Heinz, L. Urbonas and T. Gerlicher, "Effect of heat treatment method on the properties of UHPC," in *3rd Int. Symp. UHPC Nanotechnol. Constr. Mater.,*, Kassel Uni, Kassel, Germany, 2012.

[78] P. Hiremath and S. Yaragal, "Effect of different curing regimes and durations on early strength development of reactive powder concrete," *Construction and Building Materials,* vol. 154, pp. 72--87, 2017.

[79] A. Emmanuel, S. Krishnan and S. Bishnoi, "Influence of curing temperature on hydration and microstructural development of ordinary Portland cement," *Construction and Building Materials,* vol. 329, p. 127070, 2022.

[80] P. Shen, L. Lu, W. Chen, F. Wang and S. Hu, "Efficiency of metakaolin in steam cured high strength concrete," *Construction and building materials,* vol. 152, pp. 357--366, 2017.

[81] H. Hamada, A. Alattar, B. Tayeh, F. Yahaya and I. Almeshal, "Influence of different curing methods on the compressive strength of ultra-high-performance concrete: A comprehensive review," *Case Studies in Construction Materials,* vol. 17, p. 01390, 2022.

[82] D. Xu, J. Tang, X. Hu, C. Yu, F. Han, S. Sun, W. Deng and J. Liu, "The influence of curing regimes on hydration, microstructure and compressive strength of ultra-high performance concrete: A review," *Journal of Building Engineering,* p. 107401, 2023.

[83] A. Neville, Properties of concrete, Longman London, 1995.

[84] S. Allena, C. Newtson and M. Tahat, Mechanical Properties of Ultra-High Strength Concrete with Local Materials, 2012.

[85] O. Oguzhan, Y. Erem and S. Ulku, "Effect of curing regimes on the mechanical and fresh properties of steel fiber-reinforced concrete," *Architecture, Civil Engineering, Environment,* vol. 14, pp. 69--81, 2021.

[86] Z. Mo, X. Gao and A. Su, "Mechanical performances and microstructures of metakaolin contained UHPC matrix under steam curing conditions," *Construction and Building Materials,* vol. 268, p. 121112, 2021.

[87] J. T.R, "Metakaolin as a pozzolanic addition to concrete," *Structure and performance of cements,* pp. 372--398, 2002.

[88] J. Salimi, A. Ramezanianpour and M. Moradi, "Studying the effect of low reactivity metakaolin on free and restrained shrinkage of high performance concrete," *Journal of Building Engineering,* vol. 28, p. {101053, 2020.

830

831